Bioorganic Chemistry 101 (2020) 103980

Contents lists available at ScienceDirect

Bioorganic Chemistry

journal homepage: www.elsevier.com/locate/bioorg

Synthesis, pharmacological evaluation and mechanistic study of scutellarin methyl ester -4′-dipeptide conjugates for the treatment of hypoxic-ischemic encephalopathy (HIE) in rat pups

Tao Li[a,b,d,1], Dirong Wu[a,b,d,1], Yang Yang[e], Tao Xiao[a,b,d], Yilin Han[a,b,d], Jing Li[a,b,d], Ting Liu[a,b,c], Li Li[a,b], Zeqin Dai[a,b], Yongjun Li[a,c,d], Xiaozhong Fu[a,b,d,*]

[a] State Key Laboratory of Functions and Applications of Medicinal Plants, Guizhou Medical University, Guiyang 550004, Guizhou, China
[b] School of Pharmacy, Guizhou Medical University, Guiyang 550004, China
[c] Guizhou Provincial Key Laboratory of Pharmaceutics, Guizhou Medical University, Guiyang 550004, China
[d] National Engineering Research Center of Miao's Medicines & Engineering Research Center for the Development and Application of Ethnic Medicine and TCM, Ministry of Education, Guiyang 550004, Guizhou, China
[e] The Second People's Hospital of Jiangyou City, Jiangyou City 621701, Sichuan Province, China

ARTICLE INFO

Keywords:
Hypoxic-ischemic encephalopathy
Scutellarin
Oligopeptide transporter 1
Dipeptide conjugates
Pathomorphological damage

ABSTRACT

A series of novel scutellarin methyl ester-4′-dipeptide conjugates exhibiting active transport characteristics and protection against pathological damage caused by hypoxic-ischemic encephalopathy (HIE) were successfully designed and synthesized. The physiochemical properties of the obtained compounds, as well as the Caco-2 cell-based permeability and uptake into hPepT1-MDCK cells were evaluated using various analytical methods. Scutellarin methyl ester-4′-Val-homo-Leu dipeptide (**5k**) was determined as the optimal candidate with a high apparent permeability coefficient ($P_{app\ A\ to\ B}$) of $1.95 \pm 0.24 \times 10^{-6}$ cm/s, low ER ($P_{app\ BL\ to\ AP}/P_{app\ AP\ to\ BL}$) of 0.52 in Caco-2 cells, and high uptake of 25.47 μmol/mg/min in hPepT1-MDCK cells. Comprehensive mechanistic studies demonstrated that pre-treatment of PC12 cells with **5k** resulted in more potent anti-oxidative activity, which was manifested by a significant decrease in the malondialdehyde (MDA) and reactive oxygen species (ROS) levels, attenuation of the H_2O_2-induced apoptotic cell accumulation in the sub-G1 peak, and improvement in the expression of the relevant apoptotic proteins (Bcl-2, Bax, and cleave-caspase-3). Moreover, evaluation of *in vivo* neuroprotective characteristics in hypoxic-ischemic rat pups revealed that **5k** significantly reduced infarction and alleviated the related pathomorphological damage. The compound was also shown to ameliorate the neurological deficit at 48 h as well as to decrease the brain tissue loss at 4 weeks. Conjugate **5k** was demonstrated to reduce the amyloid precursor protein (APP) and β-site APP-converting enzyme-1 (BACE-1) expression. Pharmacokinetic characterization of **5k** indicated favorable druggability and pharmacokinetic properties. The conducted docking studies revealed optimal binding of **5k** to PepT1. Hydrogen bonding as well as cation-π interactions with the corresponding amino acid residues in the target active site were clearly observed. The obtained results suggest **5k** as a potential candidate for anti-HIE therapy, which merits further investigation.

1. Introduction

Brain diseases, including Alzheimer's disease (AD), vascular dementia (VD), and Parkinson's disease (PD) are accompanied by cognitive impairments, such as deficits in learning, memory, language, perception, and intellect [1]. Previous clinical and animal experiments have revealed that hypoxic-ischemic encephalopathy (HIE) is a major cause of morbidity and mortality in infants [2]. HIE affects the proper development of immature brain and subsequently leads to long-term disabilities, such as epilepsy, mental retardation, cerebral palsy, and behavioral difficulties [2–3]. Moreover, HIE causes delayed cell death via excitotoxicity, inflammation, and oxidative stress [4–7]. Thus, development of drugs able to improve brain damage and cognitive impairment caused by HIE is essential for the prevention and treatment of broad vascular cognitive impairment and dementia [8].

Scutellarin (4′,5,6-trihydroxyflavone-7-glucuronide, Scu), (Fig. 1) is

* Corresponding author at: School of Pharmacy, Guizhou Medical University, Guiyang 550004, China.
E-mail address: xiaozhong_fu@sina.com (X. Fu).
[1] Tao Li and Dirong Wu contributed equally to this work, they are the co-first authors.

https://doi.org/10.1016/j.bioorg.2020.103980
Received 11 February 2020; Received in revised form 13 April 2020; Accepted 29 May 2020
Available online 01 June 2020

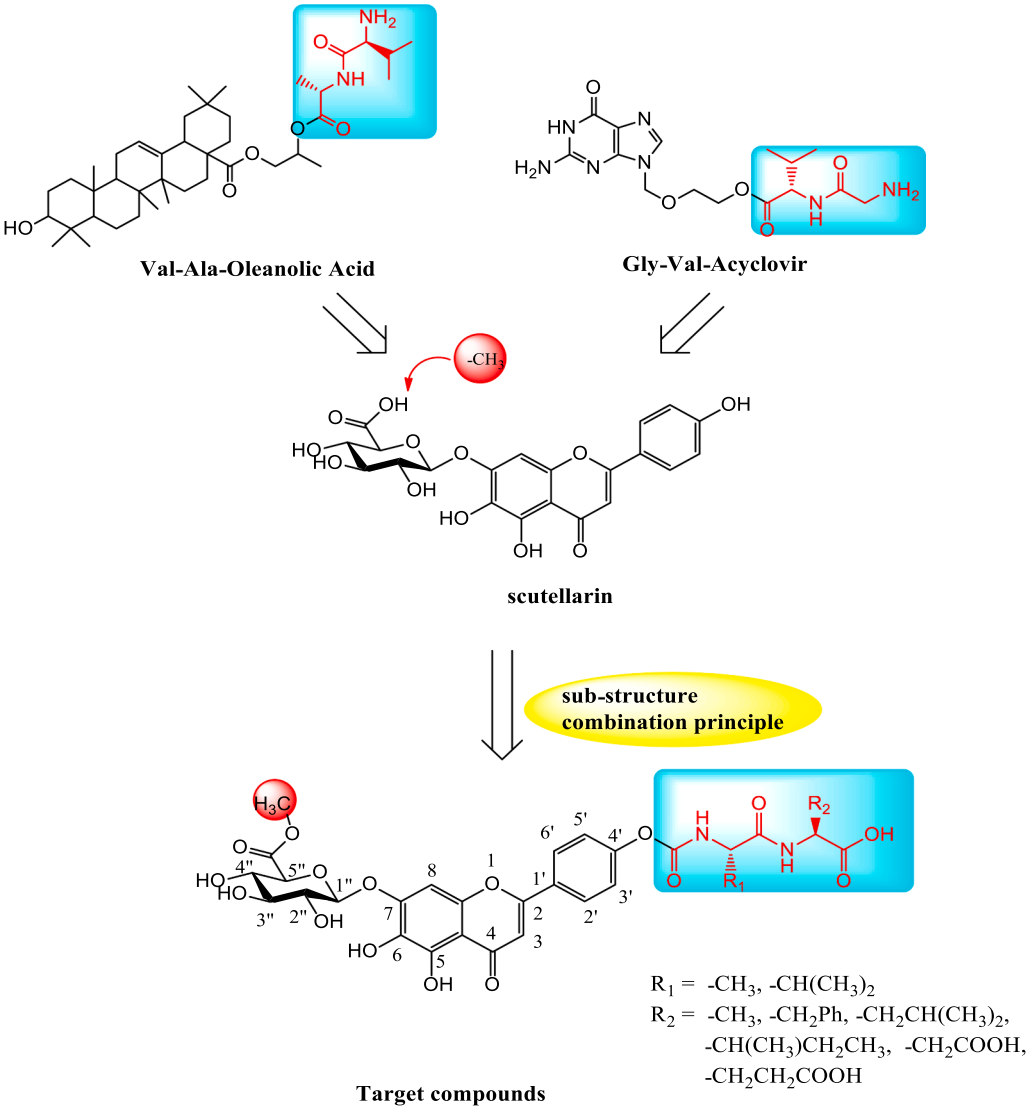

Fig. 1. Designed target compounds scutellarin methyl ester-4′-dipeptide conjugates.

an active ingredient extracted from traditional Chinese medicine *Erigeron breviscapus* (Vant) Hand–Mazz, which has been clinically used in China to treat acute cerebral infarction and paralysis induced by cerebrovascular diseases, including hypertension, cerebral thrombosis, and cerebral hemorrhage since 1984 [9–10]. So far, various studies have identified the anti-oxidative effects of scutellarin against oxidative stress caused by hydrogen peroxide, glutamate, and hypoxia [10–13]. There is also growing evidence, which suggests that scutellarin exhibits neuroprotective effects against focal cerebral ischemia induced by middle cerebral artery occlusion (MCAO). These results can be attributed to the inhibitory effects of this compound on microglial activation in neuroinflammation, as well as to anti-oxidative, anti-inflammatory, and anti-apoptotic activities [14–17]. More recently, it has been revealed that scutellarin can also ameliorate learning and memory impairment under chronic cerebral hypoperfusion induced by permanent bilateral common carotid artery occlusion (pBCAO). This observation is suggested to be a consequence of the reduction in the Aβ formation by inhibition of the amyloid precursor protein (APP) and β-site APP-converting enzyme-1 (BACE-1) production [18]. Although the above findings demonstrate that scutellarin exhibits potent protective activities against brain injury and a remarkable therapeutic potential, so far only few attempts have been made to explore utilization of scutellarin for the treatment of pathological damage in a HIE model. Accordingly, it is essential to explore whether scutellarin displays therapeutic effects in the treatment of HIE and to evaluate its underlying mechanism. The challenges of using scutellarin clinically include an unfavorable ADME profile, i.e., poor solubility in both water and lipids, low blood–brain barrier (BBB) permeability, very low absolute bioavailability, and metabolic instability [19–23].

Over the past decade, the human intestinal oligopeptide transporter 1 (PepT1), has been widely explored as a target for increasing the oral bioavailability of poorly absorbed drugs [24,25]. PepT1 is a promising and valuable target protein, responsible for the uptake of dipeptides and tripeptides. Several dipeptide-drug conjugate were synthesized, such as Gly-Val-Acyclovir, Val-Trp-Acyclovir [26], Val-Ala-Oleanolic Acid [27], Pro-Ile-Zidovudine [28] and they appeared to combine both chemical stability and good affinity for the PepT1 transporter, the peptide carrier strategy applied to improve oral absorption and bioavailability via targeting the PepT1 transporter.

In recent years, to overcome disadvantages of scutellarin, a prodrug strategy has been used to modify the structure of Scu. The approach involves introduction of long aliphatic chain; ethyl, benzyl, *N*,*N*-dialkylglycolamide ester and *N*,*N*-dialkylacetyl amino moieties to the glucuronic acid carboxyl group and the 4′-hydroxyl functionality of the compound [29–31], and previous research also revealed that the glucuronic acid carboxyl moiety and the 4′-hydroxyl group play important roles in the structural modification of Scu. Although the developed Scu

derivatives displayed good protective activity against oxidative damage and optimal absorption characteristics *in vitro*, scutellarin analogs exhibiting both improved active transportation and enhanced protective properties against the HIE impairment have not been described.

Based upon above research conclusions, in the present study, motivated by our continuing interest in exploring novel agents for the treatment of HIE, we firstly envisaged that scutellarin methyl ester-4′-dipeptide conjugates derived from scutellarin can be used as neuroprotective agents. We envisioned that the novel conjugates would display desirable protective activities against the HIE impairment and exhibit optimal active transport characteristics (Fig. 1). Herein, we report our recent findings on the design, synthesis, and biological evaluation of scutellarin methyl ester-4′-dipeptide conjugates. The prepared analogs displayed improved physiochemical properties, Caco-2 cell permeability, enhanced hPepT1-mediated transport properties, superior anti-oxidative activities *in vitro* and neuroprotective characteristics *in vivo*, as well as improved pharmacokinetic properties.

2. Results and discussion

2.1. Chemical synthesis

The procedure for the preparation of scutellarin methyl ester-4′-dipeptide conjugates (**5a–l**) is outlined in Scheme 1.

Amino acid *tert*-butyl ester hydrochlorides, such as alanine (Ala) and valine (Val) (**1a-b**) were dissolved in anhydrous CH_2C1_2. Subsequently, a solution of triphosgene [bis(trichloromethyl) carbonate] (BTC) in CH_2C1_2 was added to the initial solution at −10 °C. Following stirring at −10 °C for 2 h, the solution was washed with a cold 0.1 M aqueous solution of hydrochloric acid, dried, and concentrated *in vacuo* to obtain L-amino acid ester isocyanates **2a-b** quantitatively as light yellow oils. Scutellarin methyl ester was then coupled with **2a-b** in the presence of Et_3N in anhydrous DMF at 50 °C for 10 h under N_2 atmosphere. Subsequently, the solvent was evaporated *in vacuo* and the resulting residue was purified using routine flash column chromatography on silica gel (eluent: chloroform/methanol = 15:1–20:1 v/v) to obtain compounds **3a-b**. Intermediates **3a-b** were then deprotected using trifluoroacetic acid (TFA) at 0 °C for 5–6 h to afford **4a-b**. The scutellarin methyl ester-dipeptide conjugates (**5a-l**) were synthesized by condensation of compounds **4a-b** with L-amino acid *tert*-butyl ester hydrochlorides (e.g. Val, Phe, Glu, Asp, Leu, Ile). The reactions were carried out in the presence of peptide-coupling reagents, such as EDC or HBTU/DIPEA in anhydrous DMF at 0 °C for 0.5 h, and then at room temperature for 24 h. Finally, the deprotection reactions were carried out utilizing TFA according to the procedures described above to generate the desired target compounds. The structures of analogs **5a-l** were confirmed using $^1H/^{13}C$ nuclear magnetic resonance (NMR) spectroscopy, electrospray ionization-mass

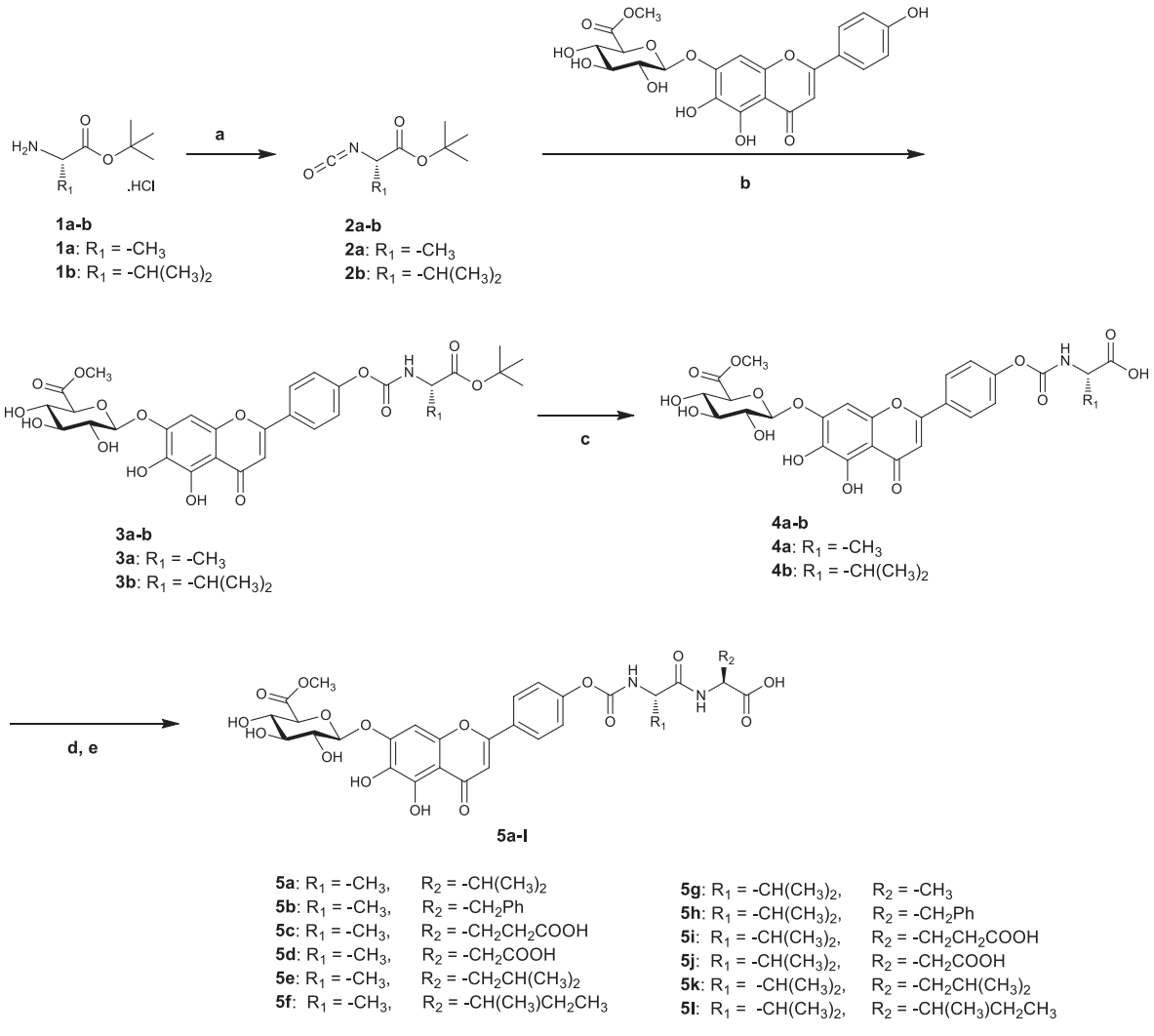

Scheme 1. Reagents and conditions: (a) bis(trichloromethyl) carbonate (BTC), pyr, DCM, −10 °C, 2 h, 1 M HCl, 90–95%; (b) anhydrous THF/DMF, Et_3N, 50 °C, 40–55%, 12 h; (c) TFA, 0 °C, 5–6 h, 29.9–44.3%; (d) amino acid *tert*-butyl ester, EDC, HBTU/DIPEA, DMF, 0 °C for 0.5 h, then room temperature for 24 h; (e) TFA, DCM, 0 °C, 5–6 h, yields for last two steps were 23.2–57.9%.

Table 1
The physicochemical properties for scutellarin methyl ester carbamate derivatives.

Compds	Aqueous solubility (μg/mL)	Fold increase	Stability in Plasma ($t_{1/2}$ min)	Stability in simulated intestinal fluid ($t_{1/2}$h)
Scu	8.52	1.0		–
5a	126.94	14.9	10	> 4
5b	167.84	19.7	10	> 4
5c	247.93	29.1	35	> 4
5d	313.53	36.8	35	> 4
5e	40.04	4.7	45	> 4
5f	351.87	41.3	35	> 2
5g	179.77	21.1	10	> 4
5h	189.14	22.2	10	> 4
5i	149.10	17.5	45	> 2
5j	253.04	29.7	40	> 4
5k	332.91	39.1	45	> 4
5l	427.70	50.2	45	> 4

spectrometry (MS-ESI) as well as high resolution mass spectrometry (HRMS-ESI) analyses. Spectral data were in accordance with the assigned structures and all of the characterization data are provided in the experimental section.

2.2. Biological evaluation

2.2.1. Physicochemical property studies

The study of the physicochemical properties of the obtained compounds (Table 1) revealed that analogs containing a free carboxyl functionality (**5c–d** and **5i-j**) or a larger steric hindrance alkyl moiety (**5e–f** and **5k-l**) in their carbamate group were significantly more stable ($t_{1/2}$ 35–45 min) in the plasma. Evaluation in artificial intestinal fluid showed that the dipeptide compounds **5a-l** exhibited good stability ($t_{1/2}$ > 4 h) in this environment. These outcomes are attributed to the increasing steric hindrance of the carbamate strand and the formation of intermolecular hydrogen bonds, which block the approach of enzymes to the carbamate linkage. With the exception of compound **5e**, aqueous solubility of all target compounds was significantly higher (126.94–427.70 μg/mL) than that of scutellarin (8.52 μg/mL). Particularly noteworthy are the solubilities of compounds **5f** (351.87 μg/mL) and **5l** (427.70 μg/mL), which were 41–50 times higher than the solubility of scutellarin. Moreover, metabolic studies using liver microsomes demonstrated that analogs **5a–l** were first converted into scutellarin methyl ester by a hydrolase enzyme before being transformed into scutellarin.

2.2.2. Caco-2 cell-based permeability assay

The Caco-2 cell permeability assay (Table 2) demonstrated that except for compound **5a** with a higher ratio of $P_{app\ BL\ to\ AP}/P_{app\ AP\ to\ BL}$ (ER 2.16) than the ratio for scutellarin (ER 1.93), the ratios of $P_{app\ BL\ to\ AP}/P_{app\ AP\ to\ BL}$ (ER) for compounds **5b-5l** were within the range of 0.52–1.63. These values are lower than the ER of scutellarin, suggesting that the efflux effect of scutellarin is higher than that of compounds **5b-5l**. Among them, ER values of **5b**, **5c**, **5f**, **5h**, **5j**, and **5l** were higher than 1.0, while ER values of **5d**, **5g**, **5i**, and **5k** were lower than 1.0. These outcomes indicate greater permeability in the basolateral plate (BL) to apical plate (AP) direction for compounds **5b**, **5c**, **5f**, **5h**, **5j**, and **5l** than for compounds **5d**, **5g**, **5i**, and **5k**. Additionally, compared with scutellarin, Caco-2 cell permeability of **5d**, **5g**, **5i**, **5j**, and **5k** considerably increased, while their $P_{app\ AP\ to\ BL}$ values were 9.7, 9.1, 9.2, 8.2, and 13.9 times higher than the $P_{app\ AP\ to\ BL}$ value of scutellarin. Among the prepared compounds, **5k** exhibits the highest $P_{app\ AP\ to\ BL}$ value ($1.95 \pm 0.24 \times 10^{-6}$ cm/s) and the lowest ER value (0.52) (Fig. 2). The initial SAR evaluation revealed that except for **5l**, substitution of Ala carbamate in compounds **5a-f** with the corresponding

Table 2
Apparent permeability coefficients (P_{app}) of scutellarin methyl ester carbamate derivatives in Caco-2 cells.

Compounds	$P_{app\ A\ to\ B} \times 10^{-6}$ (cm/s)[a]	$P_{app\ B\ to\ A} \times 10^{-6}$ (cm/s)[a]	ER ($P_{app\ B\ to\ A}$/ $P_{app\ A\ to\ B}$)[b]
Scutellarin[d]	0.14 ± 0.24[c]	0.27 ± 0.15	1.93
5a	0.31 ± 0.15	0.67 ± 0.09	2.16
5b	0.75 ± 0.11	1.17 ± 0.23	1.56
5c	0.77 ± 0.27	0.86 ± 0.22	1.12
5d	1.36 ± 0.13	1.02 ± 0.17	0.75
5f	1.09 ± 0.24	1.57 ± 0.31	1.44
5g	1.27 ± 0.19	0.89 ± 0.12	0.70
5h	1.09 ± 0.27	1.55 ± 0.27	1.42
5i	1.29 ± 0.19	0.85 ± 0.08	0.66
5j	1.15 ± 0.37	1.77 ± 0.25	1.54
5k	1.95 ± 0.24	1.02 ± 0.18	0.52
5l	0.71 ± 0.15	1.16 ± 0.21	1.63

[a] $P_{app\ A\ to\ B}$: transport of the compound from apical to basolateral; $P_{app\ B\ to\ A}$: transport of the compound from basolateral to apical

[b] ER ($P_{app\ B\ to\ A}/P_{app\ A\ to\ B}$): the ratio of $P_{app\ B\ to\ A}$ to $P_{app\ A\ to\ B}$

[c] Data are mean ± SD (n = 3)

[d] The concentration of the test compounds was at 2.0×10^{-4} M for scutellarin and 1.5×10^{-4} M for compounds **5a-l**. The incubation time was up to 120 min

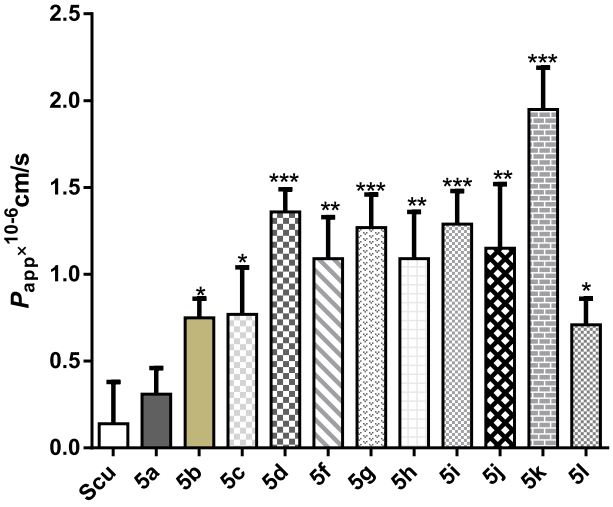

Fig. 2. The apical-to-basolateral apparent permeability coefficients ($P_{app\ AP\ to\ BL}$) of scutellarin methyl ester 4′-L-dipeptide carbamate conjugates **5a-5l** in Caco-2 cells (mean ± SD, n = 3). *p < 0.05, **p < 0.01, and ***p < 0.001 *vs.* scutellarin.

Val carbamate moieties in compounds **5g-l** significantly enhanced $P_{app\ AP\ to\ BL}$, indicating that the Val carbamate dipeptide conjugates exhibit greater potential for future applications. The obtained outcomes also demonstrated that analogs **5d**, **5g**, **5i**, and **5k** display significantly higher Caco-2 cell permeability and lower ER values than scutellarin; thus, mechanistic evaluation of the uptake of these compounds would be valuable.

2.2.3. Uptake of target compounds 5d, 5g, 5i, and 5k into hPepT1-Madin-Darby Canine Kidney (MDCK) cells

To evaluate the functionality of the cell system, protein expression of PepT1 in stably transfected hPepT1-MDCK cell lines was initially established according to a previously reported method [32]. Importantly, the identified results were consistent with the data available in the literature [33]. Fig. 3 demonstrates that the uptake rate in the hPepT1-MDCK cells for all tested prodrugs (**5d**, **5g**, **5i**, **5k**) significantly increased following the attachment of the dipeptides to the scutellarin methyl ester; however, in MDCK cells, the uptake rate for all

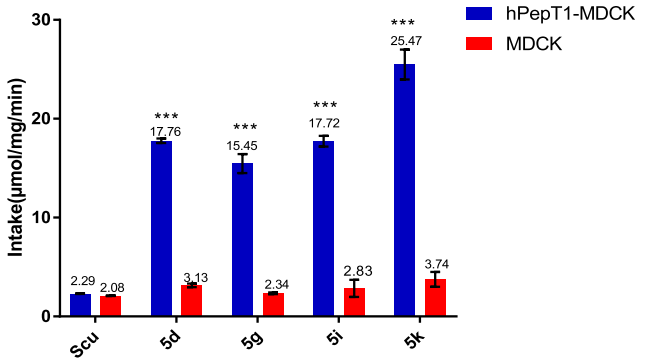

Fig. 3. The intake of scutellarin and target compounds (**5d, 5g, 5i, 5k**) in the hPepT1-MDCK and MDCK cell lines. Data are shown as mean ± SD (***p < 0.001).

compounds remained practically unchanged. Moreover, we noted that the uptake rates of Scu dipeptide derivatives **5d**, **5g**, **5i**, **5k** were significantly higher than that of Scu (***p < 0.001) in the hPepT1-MDCK cells. Among all prodrugs, **5k** (Scu-Val-Leu) exhibited the highest uptake rate of 25.74 μmol/mg/min, which was 11.2-fold higher than that of Scu. These observations strongly suggest that the introduction of the Val-Leu dipeptide into scutellarin methyl ester improves its uptake in the hPepT1-transfected MDCK cells and that analog **5k** is an optimal prodrug candidate for further evaluation.

2.2.4. Molecular docking studies of compound *5k* with PepT1

To provide insight into the molecular mechanism of oligopeptide transporter 1 (PepT1), a computational docking experiment was carried out. The binding modes of compound **5k** in stereoview are illustrated in Fig. 4. The prodrug molecules were docked into the protein binding pocket using the "Protein Preparation Wizard 2017″ workflow in the Schrödinger suite and the Force Field OPLS3 was utilized to optimize the protein, including addition of missing hydrogen atoms to form disulfide bonds. Employing the precision analysis of Schrödinger XP, the lowest energy structure was calculated and selected as the optimal conformational structure. The possible binding modes of compound **5k** with PepT1 were explored by docking the analog into the PepT1 binding cleft.

As it can be seen in Fig. 4(A), the dipeptide moiety of **5k** extends into the central cavity of binding pocket and displays an analogous binding position to the transported dipeptide substrate. Fig. 4(B) shows the fit of **5k** into active site of the transporter and a number of interactions exist between **5k** and amino acid residues of its action target. Fig. 4(C) further illustrates the binding relationship between **5k** and amino acid residues of its target. For instance, the oxygen atom of terminal leucine carboxycarbonyl and hydrogen atom of amide bond in the dipeptide structure of the compound **5k** form two hydrogen bonds with Ser404 and Ser149 residues, respectively. Moreover, the hydroxyl group at the 6 position and the oxygen atom of glycoside bond at the 7 position on the A ring of **5k** form three hydrogen bonds with Tyr68, Tyr30 and Arg26 residues of binding target, respectively. There are two additional hydrogen bonds between the 3 and 4-position hydroxyl groups of glucuronic acid and Asn156 and Glu400 residues of binding target, while the A ring of **5k** forms cation-π interaction with the Lys126 residue, respectively. The binding results are shown in Fig. 4A-C and it can be seen that compound **5k** approaches the PepT1 binding channel. It appears that compounds containing L-carbamate dipeptide groups exhibit more optimal binding activities as a result of their hydrophilic and hydrophobic properties. These observations confirmed the validity of our strategy for designing scutellarin methyl ester-4′-dipeptide conjugates as substrates for oligopeptide transporter 1 to enhance the transport efficiency.

2.2.5. In vitro anti-oxidative activities of compound *5k*

Considering that compound **5k** exhibited the highest permeability in Caco-2 cells and highest uptake in hPepT1-MDCK cells, we subsequently examined its anti-oxidative activity *in vitro* and studied the corresponding mechanisms.

*2.2.5.1. Effects of compound **5k** on LDH and MDA in PC12 cells*. Compared to Scu, pretreatment with analog **5k** at 10 and 20 μM, followed by treatment with H_2O_2 (1000 μM) attenuated the LDH activity by approximately 40% and 50%, respectively ($P < 0.05$ and $P < 0.01$ *vs.* Scu; Fig. 5A). Moreover, compared to Scu, pretreatment with **5k** at 2, 10, and 20 μM resulted in a decrease in the level of MDA in a concentration dependent manner. Particularly, at 20 μM, **5k** reduced the MDA level by approximately 30% ($P < 0.05$ *vs.* Scu; Fig. 5B).

*2.2.5.2. Effects of **5k** on the DNA condensation, intracellular ROS production, and MMP loss in PC12 cells*. Hoechst 33,342 staining confirmed that nuclear DNA condensation and nuclear fragmentation occurred following treatment with 1000 μM of H_2O_2. Pretreatment with Scu and **5k** inhibited these apoptotic features (Fig. 6A). Microscopic observation revealed that in the control group, the PC12 cells exhibited regular, rounded nuclei, as whereas nuclear pyknosis, dense staining, and a large number of apoptotic bodies indicative of apoptosis were seen after the cells were treated with H_2O_2 (Fig. 5A, arrows). Based on the analysis of the blank group, the ROS production in the H_2O_2 treatment group significantly increased to 195.22 ± 11.23%. Nevertheless, pretreatment with Scu (20 μM) reduced the ROS production to 179.06 ± 16.68% ($P < 0.05$ *vs*·H_2O_2 group), while pretreatment with **5k** (20 μM) further reduced the ROS production to 104.60 ± 9.79% ($P < 0.01$ *vs.* Scu; Fig. 6B). Furthermore, treatment of the blank group with 1,000 μM of H2O2 considerably decreased the mean fluorescence intensity of the MMP probe (Rho123) to 28.73 ± 2.53% ($^{\#\#\#}p < 0.001$ *vs.* blank; Fig. 6C-D). However, pretreatment with 20 μM of **5k** noticeably increased the mean fluorescence intensity of Rho123 to 87.38 ± 11.57% ($P < 0.05$ *vs.* Scu; Fig. 6C-D). These observations suggested that compound **5k** displays significant anti-apoptotic effects against H2O2-induced apoptosis in PC12 cells.

2.2.5.3. Cell apoptosis assay. We subsequently conducted identification of early and late apoptotic cells by Annexin-V/PI staining. As shown in Fig. 7A-B, compared with the blank group, the treatment of PC12 cells with 1000 μM of H_2O_2 for 6 h significantly increased the apoptosis rate to 34.8 ± 3.81%. Furthermore, compared with the H_2O_2 group, pretreatment with Scu or **5k** resulted in a reduction in the apoptosis rate. Especially, compared with the Scu group (22.1 ± 2.62%) at 20 μM, pretreatment with 10 μM and 20 μM of **5k** considerably reduced the apoptosis rate to 12.3 ± 1.21% and 11.7 ± 0.57%, respectively ($P < 0.05$ and $P < 0.05$ *vs.* Scu; Fig. 7A-B). To further evaluate whether H_2O_2 induced the cell death via apoptotic pathways, the percentage of apoptotic cells was measured utilizing flow cytometry. The presence of the sub-G1 peak in the flow cytometry detection is considered as an indicator of cell apoptosis. Our results demonstrated that treatment of cells with 1000 μM of H_2O_2 for 6 h notably induced the sub-G1 peak, indicating an apoptotic cell accumulation of approximately 41.26%. Additionally, scutellarin and **5k** significantly attenuated the H_2O_2-induced apoptotic cell accumulation in the sub-G1 peak (Fig. 7C). It is noteworthy that analog **5k** (20 μM) attenuated the H_2O_2-induced apoptotic cell accumulation in the sub-G1 peak to just 5.93% ($P < 0.05$ *vs.* Scu; Fig. 7C). Overall, our results imply that compound **5k** reduces apoptosis triggered by H_2O_2 in PC12 cells.

*2.2.5.4. Effect of **5k** on the expression of cleaved caspase-3, Bcl-2, and Bax levels in H_2O_2-induced PC12 cells*. Among the proteins regulating apoptosis, pro-apoptotic proteins belonging to the Bcl-2 family are

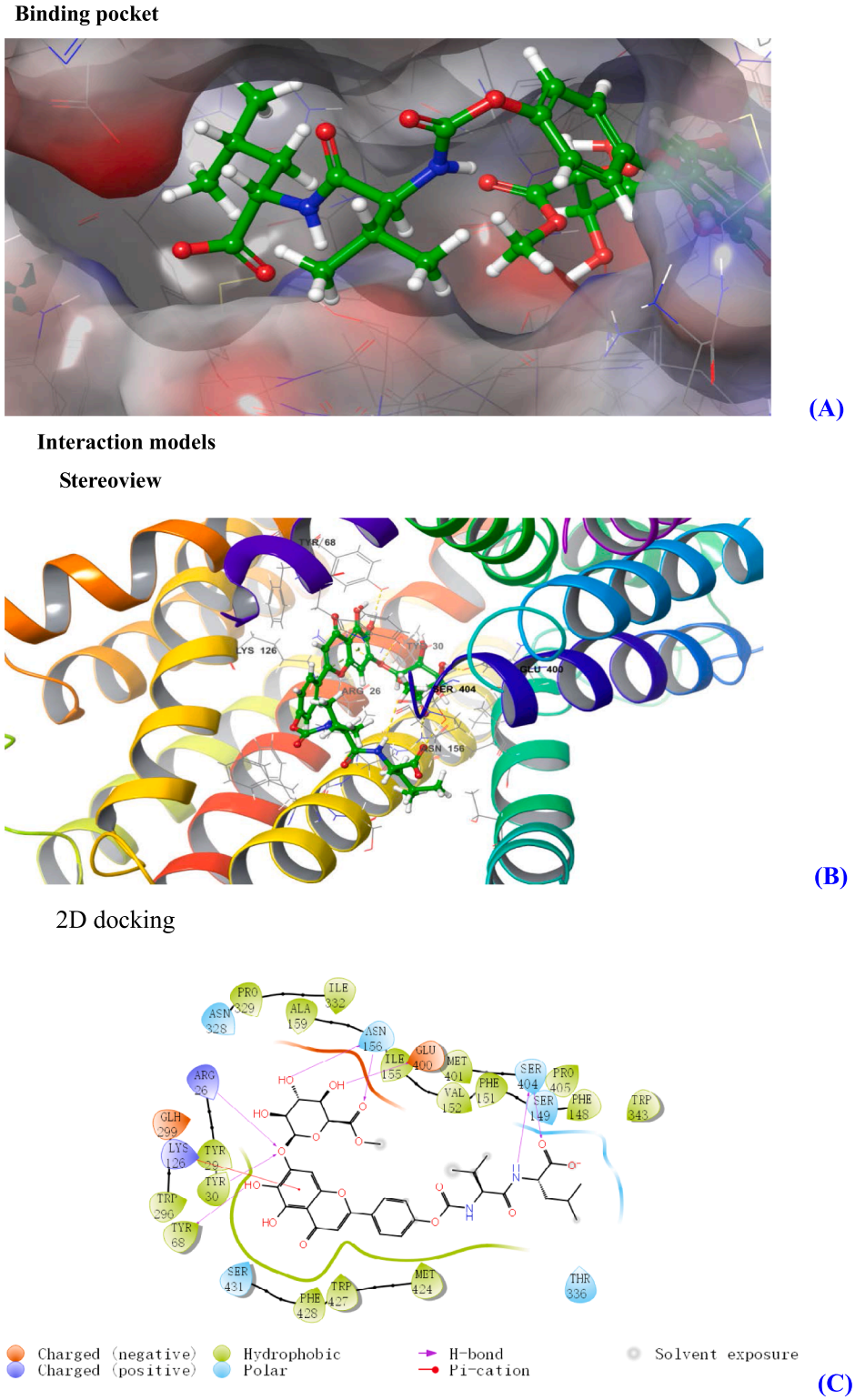

Fig. 4. Binding of compound **5k** in PepT1 (PDB ID: 4d2c): View of the optimal conformation of prodrugs binding in the cave-like binding pocket (A), the interaction modes of prodrugs in stereoview (B) and 2D display (C). The homology model structure of PepT1 (PDB ID: 4d2c) is displayed as a solid ribbon. Compound **5k** is shown in the substrate-binding pocket in the stick mode. The hydrogen bonds and cation-π interaction are shown as purple arrows and red ray, respectively. (For interpretation of the references to colour in this figure legend, the reader is referred to the web version of this article.)

recognized to play an essential role. Bax, a pro-apoptotic protein, accelerates cell death, whereas Bcl-2, an anti-apoptotic protein, suppresses cell death. Thus, the Bcl-2/Bax signaling pathway is key in the process of apoptosis [34,35]. In the present study, the treatment with compound **5k** upregulated the expression of the anti-apoptotic protein Bcl-2 (Fig. 8A). These changes caused an increase in the Bcl-2/Bax ratio. Based on the obtained results, it could be reasonably speculated that **5k** attenuates apoptosis. To further support our hypothesis, we investigated the cleave-caspase-3 activity (Fig. 8A). The analysis revealed that Scu and **5k** exhibit anti-apoptotic activities.

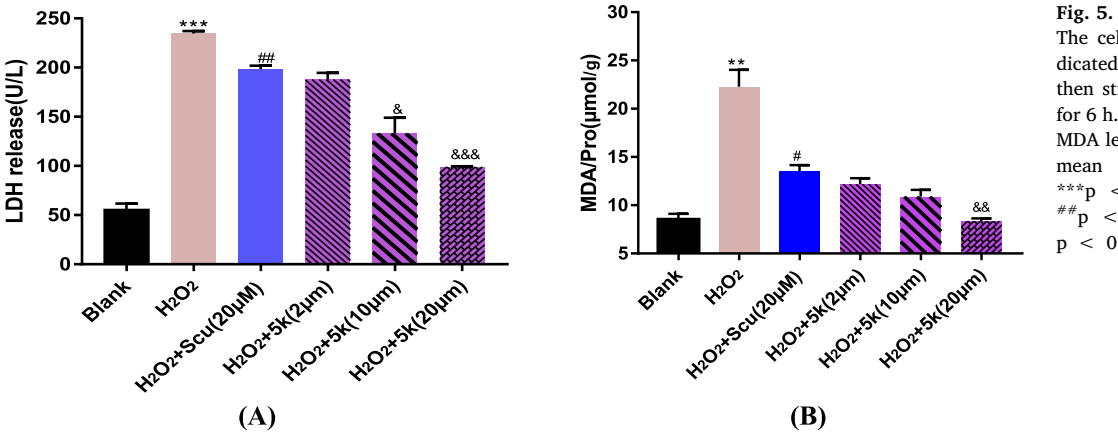

Fig. 5. Effects of **5k** on LDH and MDA. The cells were incubated with the indicated concentrations of **5k** for 24 h, then stimulated with H_2O_2 (1000 μM) for 6 h. (A) The release of LDH. (B) The MDA level. The data are represented as mean ± SEM (n = 3) $^{**}p < 0.01$, $^{***}p < 0.001$ *vs.* blank, $^{\#}p < 0.05$, $^{\#\#}p < 0.01$ *vs*·H_2O_2, $^{\&}p < 0.05$, $^{\&\&}p < 0.01$, $^{\&\&\&}p < 0.001$ *vs.* Scu.

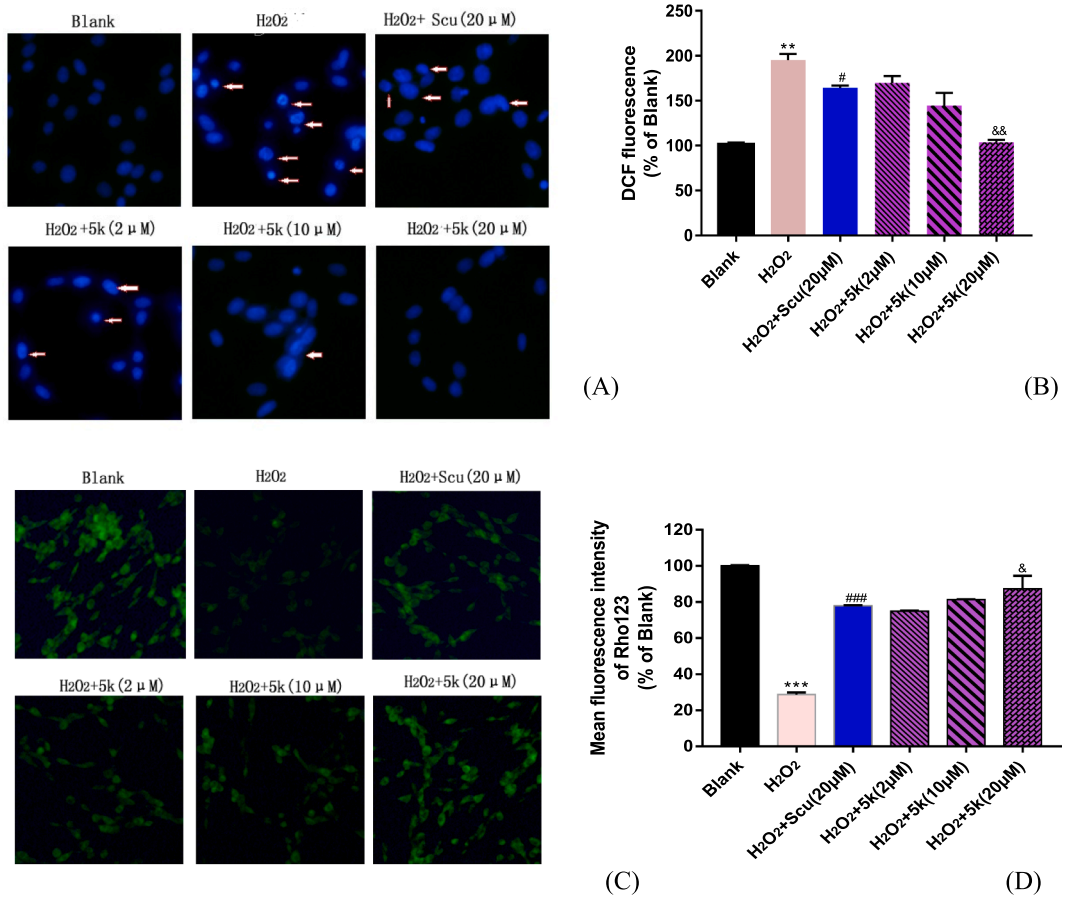

Fig. 6. Effects of **5k** on H_2O_2-induced nuclear condensation, ROS, and MMP in PC12 cells. Cells were pretreated with **5k** (2, 10, 20 μM) for 24 h and then exposed to H_2O_2 (1000 μM) for 6 h. (A) Effect of **5k** on MMP loss in H_2O_2-induced PC12 cells. (B) Effects of **5k** against H_2O_2-induced ROS production in PC12 cells. (C) Representative fluorescence images were obtained following Hoechst 33,342 staining in PC12 cells (200 ×). (D) The quantitative analysis of the mean fluorescence intensity of **5k**. The data are represented as mean ± SEM (n = 3). $^{**}p < 0.01$, $^{***}p < 0.001$ *vs.* blank, $^{\#}p < 0.05$, $^{\#\#\#}p < 0.001$ *vs*·H_2O_2, $^{\&}p < 0.05$, $^{\&\&}p < 0.01$ *vs.* Scu.

Moreover, compared with Scu (20 μM), at the same concentration, **5k** significantly increased the Bcl-2/Bax ratio ($P < 0.05$ *vs.* Scu; Fig. 8C) and attenuated the cleave-caspase-3 activation ($P < 0.01$ *vs.* Scu; Fig. 8B), which was accordance with the previous observations.

2.2.6. *In vivo neuroprotective characteristics of compound* **5k**

2.2.6.1. Effects of compound **5k** *on infarct volume, brain tissue histopathology and neurological deficits at 48 h post HIE.* The 2,3,5-triphenyltetrazolium hydrochloride (TTC) staining results demonstrated that two doses (1.3 mg and 4.4 mg/kg) of compound **5k** reduced the infarct volume compared to vehicle at 48 h post HIE. Moreover, a high dose (4.4 mg/kg) proved to be most effective, reducing the infarcted area by approximately 43% compared with the Scu group (2.8 mg/kg), suggesting that **5k** drastically reduced the infarct volume ($P < 0.05$ *vs.* Scu; Fig. 9A-B). As shown in Fig. 9C, hematoxylin-eosin (HE) staining provided a direct observation method for the analysis of the morphological characteristics of the damaged area. The investigation of the protective effects of compound **5k** on the hippocampus of the HIE rat pups revealed that in the sham group, the hippocampal pyramidal cells were abundant, compact, and normal.

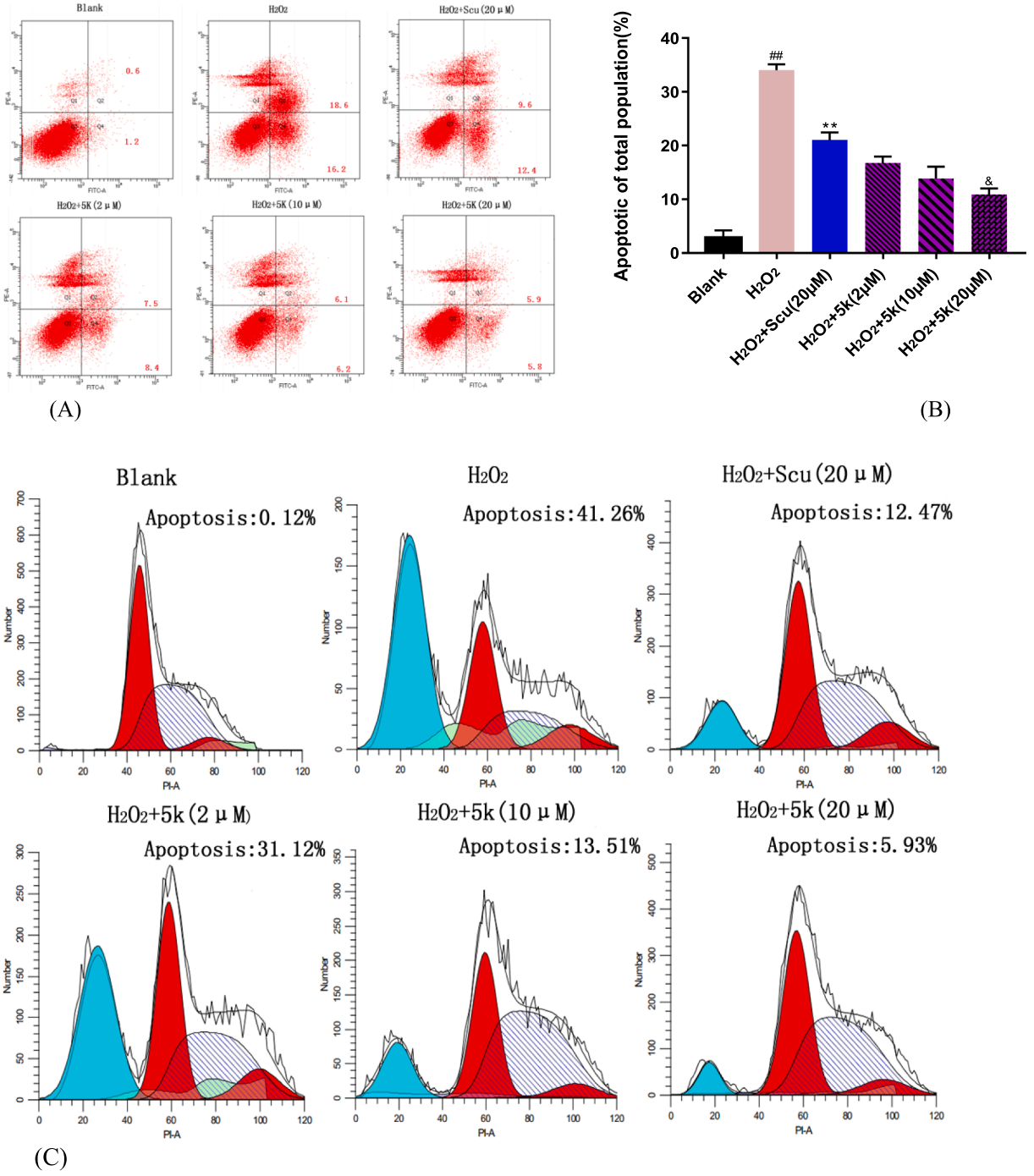

Fig. 7. The effects of **5k** on apoptosis. The cells were incubated with indicated concentrations of **5k** for 24 h, then stimulated with H_2O_2 (1000 μM) for 6 h. (A) PC12 cells were stained with Annexin-V/PI for FACS-based quantification of apoptotic cells. (B) Quantitative analysis of the apoptotic ratio. (C) The cell cycle. The data are represented as mean ± SEM (n = 3), $^{\#\#}p < 0.01$ *vs.* Blank, $^{**}p < 0.01$ *vs*·H_2O_2, $^{\&}p < 0.05$ *vs.* Scu.

Conversely, in the vehicle group, the hippocampal pyramidal cells were entirely necrosed and nuclear pyknosis, deep staining as well as fragmentation and dissolution were noted. In addition, when the HIE rat pups were pretreated with **5k** and scutellarin, the related pathomorphological damage was reduced to varying degrees. In these lesions, the group treated with compound **5k** (4.4 mg/kg) was significantly lighter than the Scu (2.8 mg/kg) group, and only a small number of pyramidal cells were necrotic. In addition, as shown in Fig. 9D, at a high dose (4.4 mg/kg), **5k** greatly ameliorated the neurological deficits compared with the scutellarin (4.4 mg/kg) pretreated HIE group ($p < 0.05$, compared with the vehicle- and sham-operated groups as well as scutellarin-treated HIE group). Moreover, the obtained results show that **5k** considerably reduced the infarct area and ameliorated the neurological deficit following cerebral HIE to different degrees. Hence, the data indicated that the prodrug of **5k** has a more potent protective effect on the ischemic injury induced by cerebral HIE in rat pups than the parent drug scutellarin.

*2.2.6.2. Effects of compound **5k** on long-term brain morphology at 4 weeks post HIE.* Representative images of the brain morphology and the microphotographs with Nissl-stained brain sections at 4 weeks post HIE are illustrated in Fig. 10A. Nissl's staining showed that the **5k**

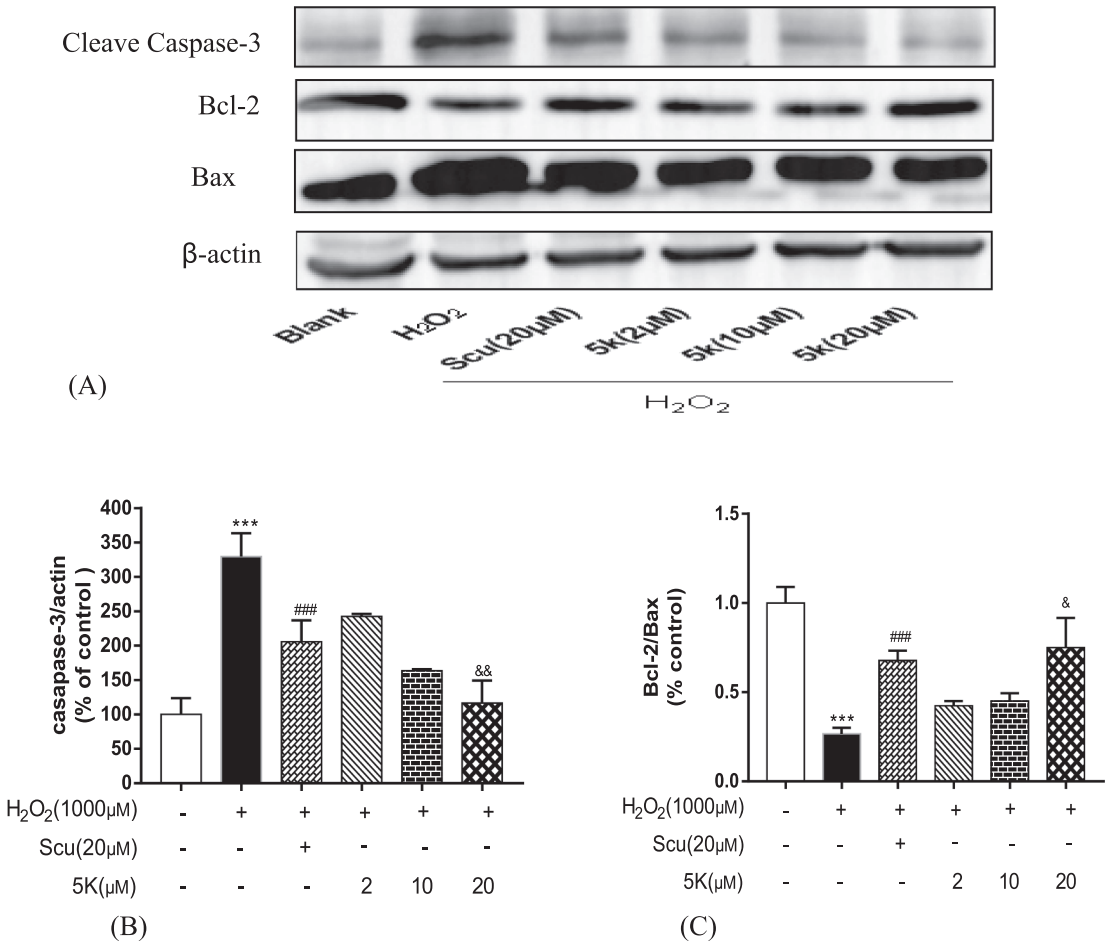

Fig. 8. Effects of **5k** on the downregulation of the Bcl-2/Bax signaling pathway induced by H_2O_2. (A) At 48 h following the H_2O_2 treatment, the protein expression levels of Bcl-2, Bax, and cleave-caspase-3 in the PC12 cells were evaluated by western blotting analysis. (B) and (C) Semi-quantified results. The outcomes are presented as the mean ± standard error of the mean and are representative of three independent experiments. ***P < 0.001 *vs.* blank, $^{\#\#\#}$p < 0.001 *vs*·H_2O_2 group, $^{\&}$p < 0.05, $^{\&\&}$p < 0.01 *vs.* Scu group.

treatment group attenuated brain tissue loss at 4 weeks post HIE. In addition, **5k** treatment significantly reduced the brain tissue loss area at 4 weeks post HIE compared to the vehicle (Fig. 10B). These observations imply that the modification of scutellarin using the dipeptide carbamate strategy significantly enhanced the protective activity of the target compounds against HIE-induced brain tissue loss. The above results may be a consequence of efficient transport through active transport carriers, such as L-type amino acid transporter 1 (LAT1) or peptide transporter 2 (PepT2), which are expressed at the BBB and in the membrane of the brain parenchymal cells. As a result, the concentration of the drug in the brain as well as its neuroprotective effects were significantly enhanced.

*2.2.6.3. Compound **5k** reduces APP and BACE-1 expression in the brain tissues of HIE- suckling rat.* Amyloid precursor protein (APP) is widely known as the precursor molecule for the generation of Aβ, while the β-site APP-converting enzyme-1 (BACE-1) is a β-secretase, which cleaves the *N*-terminal of APP to generate Aβ [36]. It has previously been reported that BACE-1 expression is upregulated in the brain tissue of AD patients and that excessive expression of this protein can cause the onset of the disease [37–38]. Based on western blot analysis, compared to the sham group, the HIE group showed significant upregulation in the expression of APP and BACE-1 in the brain tissue ($p < 0.01$ and $p < 0.001$, respectively) (Fig. 11A–C). The expression levels of APP and BACE-1 in the **5k** (1.3 mg /kg) group was not much different from those in the Scu group (Fig. 9A-C). Moreover, the **5k** (4.4 mg/kg) group exhibited significant suppression in the expression levels of APP and BACE-1 in the brain tissue ($p < 0.01$) compared to the Scu (2.8 mg/kg) group (Fig. 11A–C).

*2.2.7. Pharmacokinetic studies on **5k***

Following the injection of the tested compounds, the concentrations of scutellarin and prodrug **5k** in the blood were evaluated and the pharmacokinetic parameters were calculated. As shown in Table 3 and Fig. 12, compound **5k** exhibited a better pharmacokinetic profile than scutellarin, with significantly longer mean retention time (MRT: 17.328 ± 1.907 min) and half-life ($t_{1/2}$: 41.044 ± 25.736 min) than those of scutellarin (MRT: 9.647 ± 1.983 min; $t_{1/2}$: 7.589 ± 0.833 min). These results suggest that **5k** slowly and smoothly releases the parent drug, allowing reduced metabolic opportunities for scutellarin, and subsequently prolonging the action time of the drug. Moreover, the AUC $_{(0\text{-}t)}$ value of **5k** (66.896 ± 5.113 mg/L.min) was lower than that of scutellarin (363.568 ± 42.171 mg/L.min), while volume of distribution of **5k** (V_d: 5.876 ± 0.810 l/kg) was significantly higher than that of scutellarin (0.301 ± 0.020 l/kg). These observations could be explained by the fact that due to its 4′-dipeptide conjugate structure, **5k** is transported by active transport carriers, such as L-type amino acid transporter 1 (LAT1) or peptide transporter 2 (PepT2), which are expressed at the BBB and in the membrane of the brain parenchymal cells; therefore, **5k** is suspected to display the tendency for targeting the brain. Consequently, following the transporter-mediated delivery of **5k** across the BBB and cellular

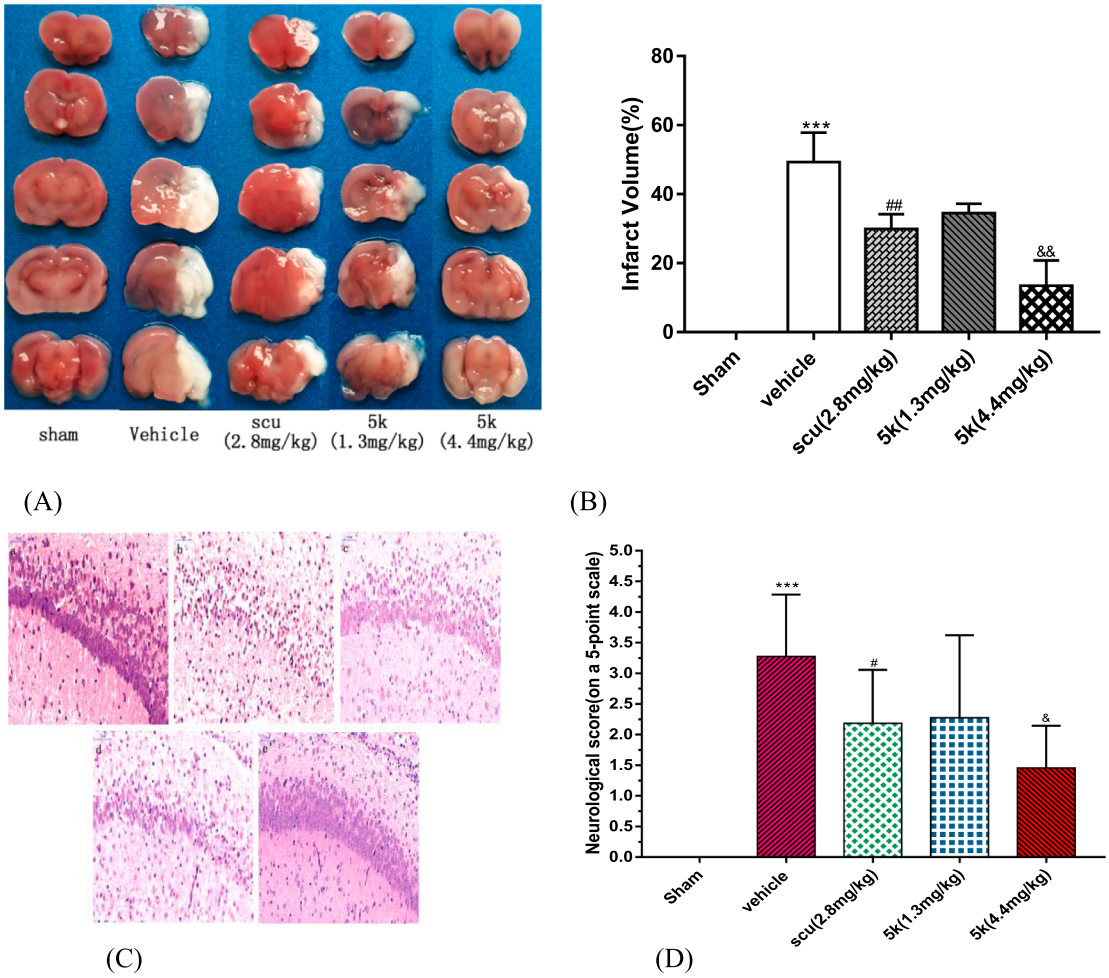

Fig. 9. Effects of compound **5k** on infarct volume and short-term neurological deficits at 48 h post HIE. Representative TTC stained brain sections (A) and TTC analysis (B) at 48 h post HIE with **5k** treatment significantly reduced the infarct volume. (C) Effects of compound **5k** on the HE staining in the HIE rat pups at 48 h. a: sham group. b: vehicle group. c: 2.8 mg/kg Scu. d: 1.3 mg/kg of **5k**. e: 4.4 mg/kg of **5k**. (D) Neurological score at 48 h post HIE with **5k** treatment showed an improvement in the outcome. Data are presented as mean ± SD. ***P < 0.001 *vs.* sham, $^{\#}$P < 0.05 *vs.* vehicle, $^{\&}$P < 0.05 *vs.* Scu, n = 6 per group. The differences between groups were evaluated by one-way ANOVA followed by Tukey's test.

membrane barrier, the parent drug will be released at its target site inside the brain parenchymal cells and as a result may lead to a decrease in the concentration of **5k** in the blood. We therefore postulate that the presence of the 4′-dipeptide fragments benefits "drug-like" molecular physicochemical properties, resulting in improved prodrug absorption, as demonstrated in both *in vitro* and *in vivo* assays.

3. Conclusions

In the current study, based on our previous research, we designed and synthesized a series of scutellarin methyl ester-4′-dipeptide conjugates. The obtained compounds were evaluated as potential anti-HIE agents. Among them, compound **5k** exhibited the most optimal $P_{app\ A\ to\ B}$, the lowest ER values in Caco-2 cells, and the highest uptake value in hPepT1-MDCK cells. Moreover, the mechanistic studies demonstrated that pre-treatment of the PC12 cells with **5k** resulted in more potent protective activity against oxidative damage by improving the relevant *in vitro* detection indicators. Analog **5k** displayed remarkable therapeutic effects in the HIE rat pups model. A reduction in the infarct area, decrease in the related pathomorphological damage, amelioration of the neurological deficits, attenuation of the brain tissue loss as well as reduction in the APP and BACE-1 expression were observed. Finally, the favorable pharmacokinetic profile of **5k** was also confirmed in the conducted *in vivo* studies. Overall, our results suggest that the scutellarin methyl ester-4′-dipeptide conjugates strategy may be used as an effective method for the design of new scutellarin prodrugs with enhanced therapeutic effects, improved absorptive potential *in vitro* and encouraging pharmacokinetic profiles. Further work on the structure–activity relationships (SAR) of these compounds is currently being carried out in our laboratory.

4. Experimental procedures

4.1. Chemical synthesis

Scutellarin (Scu, purity > 95%, HPLC) was provided by Feng shang jian Pharmaceutical Co. Ltd. (Yunnan, China). Scutellarin methyl ester was prepared according to the available literature procedures (Lu et al., 2010). All other reagents were 97–99% pure and purchased from Sinopharm Chemical Reagent Co., Ltd. (SCRC). $^{1}H/^{13}C$ nuclear magnetic resonance (NMR) spectra were recorded on a Varian Mercury 400 spectrometer. Tetramethylsilane was used as the reference and the *J* values are given in Hz. Low-resolution mass spectra were obtained utilizing an ACQUITY TQD (triple quadrupole) low-resolution mass spectrometer (Waters, America). High-resolution mass spectra were obtained using the microTOF-Q II ESI-Q-ToF LC/MS/MS apparatus

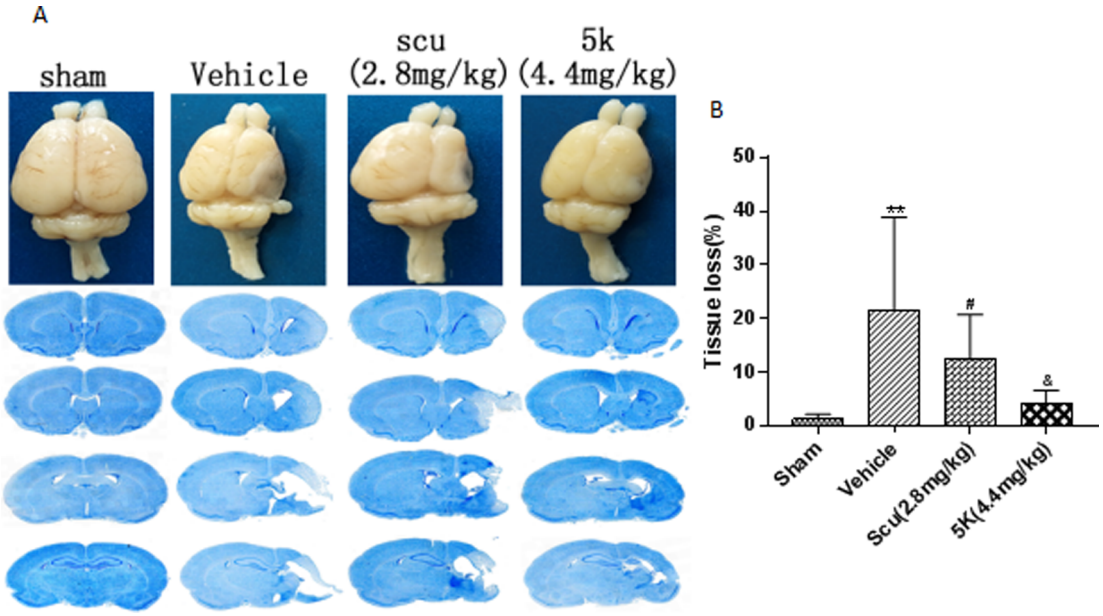

Fig. 10. Representative brain morphology images of Nissl-stained brain sections at 4 weeks post HIE. (A) Treatment with **5k** significantly reduced the percentage of tissue loss. (B) Significant reduction of the brain tissue loss area following treatment with **5k** compared to vehicle. Data are presented as mean ± SD, $^{**}P < 0.01$ *vs.* sham, $^{\#}P < 0.05$ *vs.* vehicle, $^{\&}P < 0.05$ *vs.* Scu, n = 6 per group. The differences between groups were evaluated by one-way ANOVA, followed by Tukey's test.

(Bruker Daltonics). Flash chromatography was carried out on silica gel (200–300 mesh), and chromatographic solvent ratios are expressed as volume:volume. All anhydrous solvents were distilled over CaH_2 or Na/benzophenone prior to use.

4.1.1. Procedure for the preparation of scutellarin methyl ester-4′-dipeptide conjugates

A 250 mL, three-necked, round-bottomed flask, fitted with a nitrogen inlet adapter, was charged with 2.5 mmol of $_L$-amino acid *tert*-

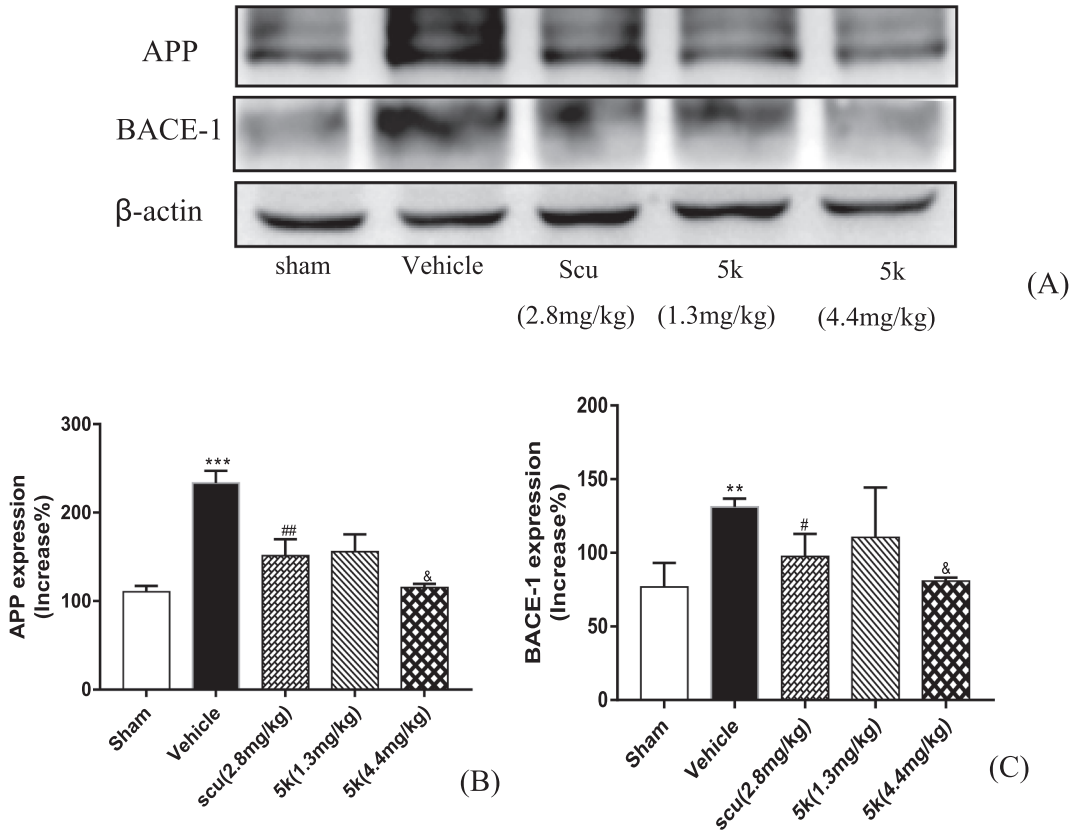

Fig. 11. Effects of scutellarin (Scu) and **5k** on APP and BACE-1 expression in the brain tissues. (A) Representative western blots illustrating differences in the band intensities of APP and BACE-1. (B) Scu and **5k** significantly attenuated the upregulation of the APP expression in the brain. (C) Scu and **5k** considerably decreased the upregulation of BACE-1 expression in the brain. Data are presented as mean ± SEM (n = 6 in each group; $^{**}p < 0.01$, $^{***}p < 0.001$ *vs.* sham, $^{\#\#}p < 0.01$, $^{\#}p < 0.05$ *vs.* vehicle, $^{\&}p < 0.05$ *vs.* Scu group).

Table 3
Pharmacokinetic parameters of scutellarin and **5k** after i.v. administration to rats (n = 6, Mean ± SD).

Parameter	Unit	Scutellarin	**5k**
AUC_{0-120}	μg/mL.min	363.56 ± 42.17	66.89 ± 5.11
MRT_{0-120}	min	9.64 ± 1.98	17.32 ± 1.90
$t_{1/2}$	min	7.58 ± 0.83	41.04 ± 25.73
V_d	L/kg	0.30 ± 0.020	5.87 ± 0.81

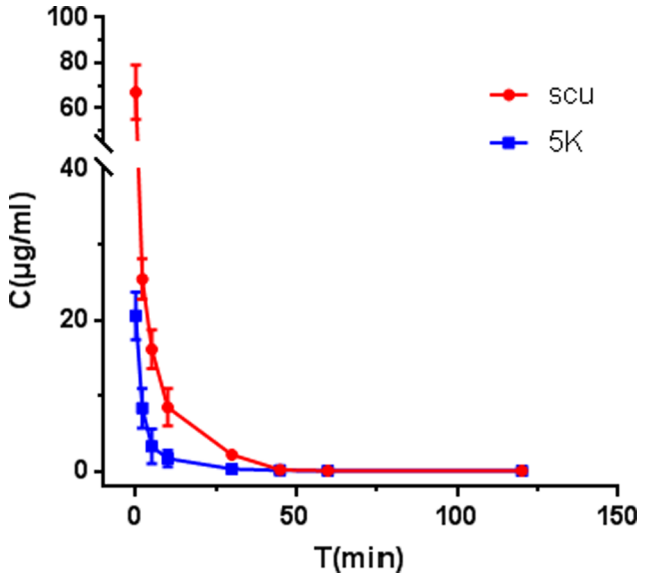

Fig. 12. Concentration profiles of scutellarin and **5k** in plasma following i.v. administration.

butyl ester hydrochloride, 50 mL of anhydrous CH_2Cl_2, and 0.8 mL (0.121 mol) of pyridine. The resulting solution was cooled at −10 °C for 30 min prior to the addition of the triphosgene [bis(trichloromethyl) carbonate] (BTC) solution (1.68 mmol in 3.0 mL of CH_2Cl_2) using a syringe over 30 s. The resulting light yellow solution was stirred at −10 °C for 2 h. The reaction mixture was then washed twice with 50 mL of a cold 0.1 M aqueous solution of HCl, ca. 30 mL of crushed ice and 20 mL of cold saturated aqueous solution of NaCl. The organic layers were separated, dried over anhydrous $MgSO_4$, filtered, and concentrated *in vacuo* to obtain L-amino acid ester isocyanate (**2a–b**) quantitatively as a light yellow oil.

Under N_2 atmosphere, scutellarin methyl ester (770 mg, 1.6 mmol) was dissolved in 15 mL of anhydrous *N*,*N*-dimethylformamide (DMF). Subsequently, a solution of compounds **2a–b** (2.43 mmol in 10 mL anhydrous THF) and Et_3N (34 μL, 0.24 mmol) was added to the mixture, and the reaction mixture was stirred at 50 °C for 10 h. Subsequently, the solvent was evaporated *in vacuo*, and the residue was purified by routine flash column chromatography on silica gel (eluent: chloroform/methanol = 15:1–20:1 v/v) to afford scutellarin methyl ester-4′-L-amino acid carbamate conjugates **3a–b**.

Compounds **3a–b** (0.22 mmol) were dissolved in trifluoroacetic acid (TFA) (3 mL) and the solution was stirred at 0 °C for 5–6 h. The reaction was monitored by thin layer chromatography (TLC) until completion. TFA was then evaporated *in vacuo*, and the resulting residue was washed with 10 mL chloroform and petroleum ether respectively using the centrifuge subside method to provide compounds **4a–b**.

1-(3-Dimethylaminopropyl)-3-ethylcarbodiimide hydrochloride (EDC) (0.254 mmol), N,*N*-Diisopropylethylamine (DIPEA) (0.305 mmol), and O-benzotriazole- *N*,*N*,*N*',*N*'-tetramethyluronium-hexafluorophosphate (HBTU) (0.508 mmol) were added to a stirred solution of compounds **4a–b** (0.254 mmol) in DMF (20 mL) at 0 °C. The reaction mixture was stirred at 0 °C for 10 min prior to the addition of L-amino acid *tert*-butyl ester hydrochloride (e.g., Val, Phe, Glu, Asp, Leu, Ile). Subsequently, the reaction mixture was stirred at room temperature for 12 h·H_2O (10 mL) and CH_2Cl_2 (10 mL) were then added and the mixture was extracted three times with CH_2Cl_2 (3 × 30 mL). The organic extracts were dried over anhydrous $MgSO_4$, filtered, and evaporated *in vacuo*. The resulting residue was purified by column chromatography on silica gel (eluent: chloroform/methanol, 35:1 v/v), followed by a deprotection with TFA/CH_2Cl_2, 10:1 (v/v) at 0 °C. The crude product was dried *in vacuo* to afford compound **5a-l** as a light yellowish-green solid. The yields were given for the last two steps of the reaction.

*4.1.2. ((4-(5,6-dihydroxy-4-oxo-7-(((2S,3S,4R,5R,6S)-3,4,5-trihydroxy-6-(methoxycarbonyl)tetrahydro-2H-pyran-2-yl)oxy)-4H-chromen-2-yl) phenoxy)carbonyl)-L-alanyl-L-valine (**5a**)*

Yield 42.1%, light yellowish green solid. ^{1}H NMR (400 MHz, DMSO-d_6) δ 10.45 (s, 1H, 6-O*H*), 8.10 (d, J = 8.7 Hz, 1H, N*H*CH$(CH_3)_2$), 8.01 (d, J = 6.9 Hz, 1H, N*H*CHCH$_3$), 7.92 (d, J = 8.7 Hz, 2H, $C_{2'6'}$–2*H*), 7.06 (s, 1H, C_3-*H*), 6.92 (d, J = 8.7 Hz, 2H,$C_{3'5'}$–2*H*), 6.87 (s, 1H, C_8-*H*), 5.29 (d, J = 7.0 Hz, 1H, $C_{\alpha'}$-*H*), 4.25–4.05 (m, 3H,$C_{2''3''4''}$–O*H*), 3.62 (s, 3H, COOC*H*$_3$), 3.34 (dt, J = 16.7, 8.7 Hz, 3H, $C_{2''3''4''}$–3*H*), 2.01 (dq, J = 13.1, 7.0, 6.6 Hz, 1H, CH(C*H*$_3$)$_2$), 1.25 (d, J = 7.0 Hz, 3H, C*H*CH$_3$), 0.82 (d, J = 4.9 Hz, 6H, CH(C*H*$_3$)$_2$). ^{13}C NMR (101 MHz, DMSO-d_6) δ 182.75, 173.53, 173.42, 169.74, 165.12, 162.00, 155.77, 153.99, 153.59, 153.17, 129.18(2C), 124.05, 121.52, 116.56(2C), 106.04, 103.40, 99.77, 93.91, 75.70, 73.22, 71.87, 57.48, 55.44, 52.56, 50.54, 30.42, 19.55, 18.48, 18.34. HRESIMS *m/z* (pos): 691.1982 $C_{31}H_{34}N_2O_{16}$ (calcd. 691.1987).

*4.1.3. ((4-(5,6-dihydroxy-4-oxo-7-(((2S,3S,4R,5R,6S)-3,4,5-trihydroxy-6-(methoxycarbonyl)tetrahydro-2H-pyran-2-yl)oxy)-4H-chromen-2-yl) phenoxy)carbonyl)-L-alanyl-L-phenylalanine (**5b**)*

Yield 45.9%, light yellowish green solid. ^{1}H NMR (400 MHz, DMSO-d_6) δ 10.46 (s, 1H, 6-O*H*), 8.27 (d, J = 7.8 Hz, 1H, -N*H*CH$_2$Ph), 7.96 (s, 1H, N*H*CHCH$_3$), 7.93 (d, J = 8.7 Hz, 2H, $C_{2'6'}$–2*H*), 7.46 – 7.07 (m, 6H, Ph-*H*), 7.06 (s, 1H, C_3-*H*), 6.92 (d, J = 8.8 Hz, 2H, $C_{3'5'}$–2*H*), 6.88 (s, 1H, C_8-*H*), 5.52 (d, J = 5.2 Hz, 1H,$C_{1'}$-*H*), 5.42 – 5.13 (m, 3H, $C_{2'3'4'}$–O*H*), 4.42 (q, J = 7.8 Hz, 1H, C*H*CH$_2$Ph), 4.18 (d, J = 9.3 Hz, 1H, $C_{5'}$-*H*), 4.09 (p, J = 7.1 Hz, 1H,C*H*CH$_3$), 3.63 (s, 3H, COOC*H*$_3$), 3.04 – 2.83 (m, 2H,C*H*$_2$Ph), 1.22 (d, J = 7.1 Hz, 3H,C*H*$_3$). ^{13}C NMR (101 MHz, DMSO-d_6) δ 182.76, 173.12 (d, J = 13.0 Hz), 169.74, 165.13, 162.01, 155.81, 153.75 (d, J = 43.3 Hz), 153.53, 153.15, 137.73, 129.78 (2C), 129.20, 128.74 (2C), 127.01, 124.11, 121.52 , 116.57 (2C), 106.06, 103.42, 99.98, 94.03, 75.76, 73.22 (2C), 71.86, 55.47, 53.97, 52.57, 50.59, 37.22, 28.01, 18.77. HRESIMS *m/z* (pos): 739.1982 $C_{35}H_{34}N_2O_{16}$ (calcd. 739.1987).

*4.1.4. ((4-(5,6-dihydroxy-4-oxo-7-(((2S,3S,4R,5R,6S)-3,4,5-trihydroxy-6-(methoxycarbonyl)tetrahydro-2H-pyran-2-yl)oxy)-4H-chromen-2-yl) phenoxy)carbonyl)-L-alanyl-L-glutamic acid (**5c**)*

Yield 35.0%, light yellowish green solid. ^{1}H NMR (400 MHz, DMSO-d_6) ^{1}H NMR (400 MHz, DMSO-d_6) δ8.22 (d, J = 7.9 Hz, 1H, –N*H*CH$_2$COOH), 8.01 (d, J = 7.2 Hz, 1H, N*H*CHCH$_3$), 7.92(d, J = 8.8 Hz, 2H, $C_{2'6'}$–2*H*), 7.06 (s, 1H, C_3-*H*), 6.92 (m, 2H, $C_{3'5'}$–2*H*), 6.86 (s, 1H, C_8-*H*), 5.29 (d, J = 6.8 Hz, 1H, $C_{1'}$-*H*), 4.24 – 4.14 (m, $C_{5'}$-H, NHC*H*CHCH$_3$), 4.07 (p, J = 7.1 Hz, 1H), 3.62 (s, 3H, COOC*H*$_3$),2.28 – 2.20 (m, 2H, CH$_2$C*H*$_2$COOH), 1.93 (tq, J = 16.1, 7.9, 7.4 Hz, 3H), 1.25 (d, J = 7.2 Hz, 3H, C*H*$_3$). ^{13}C NMR (101 MHz, DMSO-d_6) δ 182.75, 174.37, 173.66, 173.20, 169.73, 165.12, 161.99, 155.79, 154.00, 153.62, 153.16, 129.19(2C), 124.08, 121.56, 116.57(2C), 106.08, 103.44, 99.96, 94.00, 75.75, 73.22, 71.84, 52.56, 51.74, 50.64, 49.13, 30.65, 26.98, 18.50. HRESIMS *m/z* (pos): 721.1728 $C_{31}H_{32}N_2O_{18}$ (calcd. 721.1726).

*4.1.5. ((4-(5,6-dihydroxy-4-oxo-7-(((2S,3S,4R,5R,6S)-3,4,5-trihydroxy-6-(methoxycarbonyl)tetrahydro-2H-pyran-2-yl)oxy)-4H-chromen-2-yl) phenoxy)carbonyl)-L-alanyl-L-aspartic acid (**5d**)*

Yield 23.2%, light yellowish green solid. ^{1}H NMR (400 MHz, DMSO-d_6) δ 10.42 (s, 1H, 6-O*H*), 8.28 (d, J = 8.1 Hz, 1H,–N*H*CH_2COOH), 7.96 (d, J = 8.0 Hz, 1H, N*H*CHCH$_3$), 7.93 (d, J = 8.9 Hz, 2H, $C_{2'6'}$–2*H*), 7.05 (s, 1H, C_3-*H*), 6.92 (d, J = 8.8 Hz, 2H, $C_{3'5'}$–2*H*), 6.86 (s, 1H, C_8-*H*), 5.29 (d, J = 6.9 Hz, 1H, $C_{1''}$-*H*), 4.54 (q, J = 6.2 Hz, 1H, C*H*CH_2COOH), 4.18 (d, J = 9.4 Hz, 1H, $C_{5''}$-*H*), 4.12 – 4.06 (m, 1H, C*H*CH$_3$), 3.63 (s, 3H, COOC*H*$_3$), 2.71 – 2.53 (m, 2H, C*H*$_2$COOH), 1.26 (d, J = 7.0 Hz, 3H, C*H*$_3$). ^{13}C NMR (101 MHz, DMSO-d_6) δ 182.74, 172.91, 172.78, 172.17, 169.69, 165.14, 162.01, 155.81, 153.98, 153.59, 153.16, 129.19(2C), 124.15, 121.55, 116.58(2C), 106.09, 103.45, 100.10, 94.07, 75.79(2C), 73.28, 71.83, 52.55, 50.60, 49.00, 36.52, 18.74. HRESIMS *m/z* (pos): 707.1570 $C_{30}H_{30}N_2O_{18}$ (calcd. 707.1572).

*4.1.6. ((4-(5,6-dihydroxy-4-oxo-7-(((2S,3S,4R,5R,6S)-3,4,5-trihydroxy-6-(methoxycarbonyl)tetrahydro-2H-pyran-2-yl)oxy)-4H-chromen-2-yl) phenoxy)carbonyl)-L-alanyl-L-leucine(**5e**)*

Yield 46.0%, light yellowish green solid. ^{1}H NMR (400 MHz, Methanol-d_4) δ 7.82 (d, J = 6.7 Hz, 2H, $C_{2'6'}$–2*H*), 6.89 (d, J = 8.7 Hz, 2H, $C_{3'5'}$–2*H*), 6.62 (s, 1H, C_8-*H*), 5.21 (d, J = 7.3 Hz, 1H, $C_{1''}$-*H*), 4.43 (dd, J = 10.0, 5.0 Hz, 1H, C*H*CH_2CH(CH$_3$)$_2$), 4.19 (q, J = 7.0, 5.4 Hz, 2H, C*H*CH$_3$, $C_{5''}$–O*H*), 3.74 (s, 3H, COOC*H*$_3$), 3.68 – 3.52 (m, 4H, $C_{2'',3'',4'',5''}$-4*H*), 1.71 (dq, J = 13.0, 6.7 Hz, 1H, C*H*(CH$_3$)$_2$), 1.65 – 1.55 (m, 2H, CH_2CH(CH$_3$)$_2$), 1.43 (d, J = 7.1 Hz, 3H, CHCH$_3$), 0.91 (dd, J = 11.5, 6.5 Hz, 6H, CH(C*H*$_3$)$_2$. ^{13}C NMR (101 MHz, Methanol-d_4) δ 182.83, 174.98, 174.15, 169.48, 165.69, 161.67, 155.49, 154.52, 154.23, 152.99, 128.36(2C), 123.94, 121.58, 115.72(2C), 106.08, 102.57, 100.22, 93.85, 75.46, 75.40, 72.98, 71.46, 51.65, 51.05, 50.75, 40.34, 24.62, 22.12, 20.68, 16.80. HRESIMS *m/z* (pos): 705.2148 $C_{32}H_{36}N_2O_{16}$(calcd. 705.2143)

*4.1.7. ((4-(5,6-dihydroxy-4-oxo-7-(((2S,3S,4R,5R,6S)-3,4,5-trihydroxy-6-(methoxycarbonyl)tetrahydro-2H-pyran-2-yl)oxy)-4H-chromen-2-yl) phenoxy)carbonyl)-L-alanyl-L-alloisoleucine (**5f**)*

Yield 44.8%, light yellowish green solid. ^{1}H NMR (400 MHz, DMSO-d_6) δ 10.43 (s, 1H, 6-O*H*), 8.09 – 8.03 (d, 1H, N*H*CHCOOH), 8.00 (d, J = 7.1 Hz, 1H, N*H*CHCH$_3$), 7.93 (d, J = 8.8 Hz, 2H, $C_{2'6'}$–2*H*), 7.06 (s, 1H, C_3-*H*), 6.92 (d, J = 8.8 Hz, 2H, $C_{3'5'}$–2*H*), 6.87 (s, 1H, C_8-*H*), 5.29 (d, J = 7.1 Hz, 1H, $C_{1''}$-*H*), 4.24 – 4.08 (m, 3H, $C_{5''}$-H, NHC*H*CH$_3$, NHC*H*COOH), 3.62 (s, 3H, COOC*H*$_3$), 1.73 (dp, J = 13.1, 6.7 Hz, 1H, C*H*(CH$_3$)CH$_2$CH$_3$), 1.40 – 1.29 (m, 1H, CH(CH$_3$)C*H*$_2$CH$_3$), 1.24 (d, J = 7.1 Hz, 3H, CHC*H*$_3$), 1.20 – 1.05 (m, 1H, CH(CH$_3$)C*H*$_2$CH$_3$), 0.79 (t, J = 7.4 Hz, 6H, CH(C*H*$_3$)CH$_2$C*H*$_3$). ^{13}C NMR (101 MHz, DMSO-d_6) δ 182.75, 173.42, 173.35, 169.74, 165.12, 162.00, 155.78, 153.99, 153.58, 153.18, 129.19(2C), 124.08, 121.54, 116.57(2C), 106.04, 103.43, 99.79, 93.95, 75.73, 73.22, 71.87, 56.82, 55.46, 52.56, 50.51, 36.94, 25.04, 18.50, 16.01, 11.98. HRESIMS *m/z* (pos): 705.2151 $C_{32}H_{36}N_2O_{16}$ (calcd. 705.2143).

*4.1.8. ((4-(5,6-dihydroxy-4-oxo-7-(((2S,3S,4R,5R,6S)-3,4,5-trihydroxy-6-(methoxycarbonyl)tetrahydro-2H-pyran-2-yl)oxy)-4H-chromen-2-yl) phenoxy)carbonyl)-L-valylalan-ine(**5g**)*

Yield 44.8%, light yellowish green solid. ^{1}H NMR (400 MHz, DMSO-d_6) δ 8.33 (d, J = 7.0 Hz, 1H, N*H*CHCH$_3$), 7.92 (d, J = 8.8 Hz, 2H, $C_{2'6'}$–2*H*), 7.77 (d, J = 8.1 Hz, 1H, N*H*CH(CH$_3$)$_2$), 7.05 (s, 1H,C_3-*H*), 6.92 (d, J = 8.8 Hz, 2H,$C_{3'5'}$–2*H*), 6.86 (s, 1H, C_8-*H*), 5.29 (d, J = 6.9 Hz, 1H, $C_{1''}$-*H*), 4.22 (q, J = 7.1 Hz, 1H, C*H*CH$_3$), 4.17 (d, J = 9.2 Hz, 1H, $C_{3''}$–O*H*), 3.90 – 3.84 (m, 1H, C*H*(CH$_3$)$_2$), 3.63 (s, 3H, COOC*H*$_3$), 3.34 (dt, J = 17.1, 8.5 Hz, 3H, $C_{2''3''4''}$–3*H*), 1.98 (dq, J = 13.1, 6.4 Hz, 1H, CH(C*H*$_3$)$_2$), 1.25 (d, J = 7.2 Hz, 3H,CHC*H*$_3$), 0.99 – 0.85 (m, 6H, CH(C*H*$_3$)$_2$). ^{13}C NMR (101 MHz,) δ 182.75, 174.49, 171.40, 169.63, 165.14, 161.99, 155.90, 153.95, 153.19, 129.16(2C), 124.21, 121.54, 117.06, 116.55, 114.19, 106.08, 103.42, 100.19, 94.03, 78.97, 75.77, 73.30, 71.80, 60.65, 52.51, 47.99, 31.29, 19.61, 18.79, 17.60. HRESIMS *m/z* (pos): 691.1990 $C_{31}H_{34}N_2O_{16}$ (calcd. 691.1987).

*4.1.9. (S)-2-((S)-2-(((4-(5,6-dihydroxy-4-oxo-7-(((2S,3S,4R,5R,6S)-3,4,5-trihydroxy-6-(methoxycarbonyl)tetrahydro-2H-pyran-2-yl)oxy)-4H-chromen-2-yl)phenoxy)carbonyl)amino)-3-methylbutanamido)-3-phenylpropanoic acid (**5h**)*

Yield 40.5%, light yellowish green solid. ^{1}H NMR (400 MHz, DMSO-d_6) δ 10.46 (s, 1H, 6-O*H*), 8.35 (d, J = 7.3 Hz, 1H, -N*H*CH_2Ph), 7.93 (d, J = 8.4 Hz, 2H, $C_{2'6'}$–2*H*), 7.72 (d, J = 8.7 Hz, 1H, N*H*CHCH$_3$), 7.22 (d, J = 5.6 Hz, 4H, Ph-*H*), 7.16 (d, J = 6.1 Hz, 1H, Ph_4-*H*), 7.06 (s, 1H, C_3-*H*), 6.92 (d, J = 8.4 Hz, 2H, $C_{3'5'}$–2*H*), 6.88 (s, 1H, C_8-*H*), 5.50 (d, J = 5.7 Hz, 1H,), 5.30 (d, J = 5.9 Hz, 1H, $C_{1''}$-*H*), 4.43 (q, J = 7.5 Hz, 1H, C*H*CH_2Ph), 4.17 (d, J = 8.8 Hz, 1H, $C_{5''}$-*H*), 3.90 (t, J = 7.9 Hz, 1H, C*H*CH$_3$), 3.62 (s, 3H, COOC*H*$_3$), 2.93 (ddd, J = 44.6, 13.9, 7.4 Hz, 2H, C*H*$_2$Ph), 1.94 (dq, J = 12.2, 5.9, 5.5 Hz, 1H, C*H*(CH$_3$)$_2$), 0.85 (d, J = 6.4 Hz, 6H, CH(C*H*$_3$)$_2$). ^{13}C NMR (101 MHz, DMSO-d_6) δ 182.78, 173.28, 171.56, 169.67, 165.13, 162.02, 155.96, 153.94, 153.22, 137.82, 129.69(2C), 129.20, 128.75(4C), 127.01, 124.23, 121.53, 116.57(2C), 106.07, 103.41, 100.13, 94.07, 75.83, 75.75, 73.26, 71.80, 60.62, 54.01, 52.56, 37.30, 32.07, 19.61, 18.61. HRESIMS *m/z* (pos): 767.2300 $C_{37}H_{38}N_2O_{16}$(calcd. 767.2300).

*4.1.10. (S)-2-((S)-2-(((4-(5,6-dihydroxy-4-oxo-7-(((2S,3S,4R,5R,6S)-3,4,5-trihydroxy-6-(methoxycarbonyl)tetrahydro-2H-pyran-2-yl)oxy)-4H-chromen-2-yl)phenoxy)carbonyl)amino)-3-methylbutanamido) pentanedioic acid (**5i**)*

Yield 36.4%, light yellowish green solid. ^{1}H NMR (400 MHz, DMSO-d_6) δ 8.30 (d, J = 7.4 Hz, 1H, –N*H*CH_2COOH), 7.89 (d, J = 8.8 Hz, 2H, $C_{2'6'}$–2*H*), 7.82 (d, J = 8.6 Hz, 1H, N*H*CHCH$_3$), 7.03 (s, 1H, C_3-*H*), 6.90 (d, J = 8.8 Hz, 2H, $C_{3'5'}$–2*H*), 6.81 (s, 1H, C_8-*H*), 5.28 (d, J = 6.8 Hz, $C_{1''}$-*H*), 4.24 – 4.18 (m, 1H, NHC*H*COOH), 4.16 (d, J = 9.1 Hz, 1H, NHC*H*CHCH$_3$), 3.61 (s, 3H, COOC*H*$_3$), 3.36–3.30 (m, 3H, $C_{2''3''4''}$–3H), 2.32 – 2.18 (m, 2H, CH_2C*H*$_2$COOH), 2.01 – 1.87 (m, 2H, C*H*$_2$CH$_2$COOH), 1.78 (ddd, J = 11.5, 9.2, 6.4 Hz, 1H, C*H*(CH$_3$)$_2$), 0.91 (t, J = 7.2 Hz, 6H, CH(C*H*$_3$)$_2$). ^{13}C NMR (101 MHz,) δ 182.74, 174.33, 173.60, 171.79, 169.66, 165.12, 161.97, 155.88, 154.01, 153.92, 153.17, 129.19(2C), 124.16, 121.52, 116.56(2C), 106.06, 103.40, 100.03, 94.00, 75.74, 73.23, 71.78, 60.64, 52.56, 51.78, 31.28, 30.56, 29.53, 26.73, 19.63, 18.74. HRESIMS *m/z* (pos): 749.2036 $C_{33}H_{37}N_2O_{18}$(calcd. 749.2041).

*4.1.11. (S)-2-((S)-2-(((4-(5,6-dihydroxy-4-oxo-7-(((2S,3S,4R,5R,6S)-3,4,5-trihydroxy-6-(methoxycarbonyl)tetrahydro-2H-pyran-2-yl)oxy)-4H-chromen-2-yl)phenoxy)carbonyl)amino)-3-methylbutanamido)succinic acid (**5j**)*

Yield 32.0%, light yellowish green solid. ^{1}H NMR (400 MHz, DMSO-d_6) δ 8.39 (d, J = 7.0 Hz, 1H, N*H*CH_2COOH), 7.93 (d, J = 8.7 Hz, 2H, $C_{2'6'}$–2*H*), 7.79 (d, J = 8.0 Hz, 1H, N*H*CHCH$_3$), 7.06 (s, 1H, C_3-*H*), 6.92 (d, J = 8.7 Hz, 2H, $C_{3'5'}$–2*H*), 6.87 (s, 1H, C_8-*H*), 5.29 (d, J = 6.5 Hz, 1H, $C_{1''}$-*H*), 4.53 (q, J = 6.6 Hz, 1H, C*H*CH$_2$COOH), 4.16 (d, J = 9.1 Hz, 1H, $C_{5''}$-*H*), 4.12 – 3.94 (m, 1H, C*H*CH(CH$_3$)$_2$), 3.91 (t, 1H, J = 7.7 Hz, $C_{3''}$–O*H*), 3.62 (s, 3H, COOC*H*$_3$), 3.41 – 3.22 (m, 3H, $C_{2''3''4''}$–3*H*), 2.61 (qd, J = 16.8, 6.3 Hz, 2H, C*H*$_2$COOH), 1.97 (dq, J = 20.1, 6.4 Hz, 1H, C*H*(CH$_3$)$_2$), 0.90 (t, J = 7.4 Hz, 6H,CH(C*H*$_3$)$_2$). ^{13}C NMR (101 MHz, DMSO-d_6) δ 182.74, 172.79, 172.17, 171.33, 169.64, 165.11, 161.98, 155.90, 154.01, 153.92, 153.17, 129.18(2C), 124.21, 121.50, 116.55(2C), 106.05, 103.38, 100.15, 94.04, 75.77(2C), 73.24, 71.76, 60.53, 52.54, 49.02, 36.47, 31.55, 19.59, 18.54. HRESIMS *m/z* (pos): 735.1887 $C_{32}H_{34}N_2O_{18}$(calcd. 735.1885).

*4.1.12. ((4-(5,6-dihydroxy-4-oxo-7-(((2S,3S,4R,5R,6S)-3,4,5-trihydroxy-6-(methoxycarbonyl)tetrahydro-2H-pyran-2-yl)oxy)-4H-chromen-2-yl)phenoxy)carbonyl)-L-valyl-L-leucine (**5k**)*

Yield 57.9%, light yellowish green solid. ^{1}H NMR (400 MHz,) δ 8.21

(d, J = 7.4 Hz, 1H, N*H*CHCOOH), 7.89 (d, J = 8.8 Hz, 2H, $C_{2'6'}$–2*H*), 7.77 (d, J = 8.7 Hz, 1H, N*H*CH), 7.03 (s, 1H, C_3-*H*), 6.90 (d, J = 8.8 Hz, 2H, $C_{3'5'}$–2*H*), 6.82 (s, 1H, C_8-*H*), 5.28 (d, J = 6.5 Hz, 1H, $C_{1''}$-*H*), 4.22 – 4.17 (m, 1H, C*H*CH_2CH$(CH_3)_2$), 4.16 (d, J = 9.1 Hz, 1H, C*H*CH_3), 3.93 – 3.84 (m, 1H, NHC*H*-CH$(CH_3)_2$), 3.61 (s, 3H, COOC*H*$_3$), 3.33 (dq, J = 14.4, 7.8, 6.4 Hz, 3H, $C_{2''3''4''}$–3*H*), 1.99 (dq, J = 13.6, 7.0 Hz, 1H, C*H*$(CH_3)_2$), 1.68 – 1.55 (m, 1H, CHCH_2C*H*$(CH_3)_2$), 1.54 – 1.33 (m, 2H, CHCH_2CH$(CH_3)_2$), 0.90 (t, J = 7.3 Hz, 6H, CH(CH_3)$_2$), 0.83 (d, J = 6.5 Hz, 3H, CHCH_2CHCH_3), 0.78 (d, J = 6.5 Hz, 3H, CHCH_2CHCH_3). ^{13}C NMR (101 MHz, DMSO-d_6): δ 182.76, 174.48, 171.58, 169.67, 165.11, 161.99, 155.90, 153.92(2C), 153.21, 129.18(2C), 124.25, 121.52, 116.56(2C), 106.04, 103.40, 99.98, 94.02, 75.84, 75.73, 73.23, 71.80, 60.65, 52.55, 50.86, 31.33, 29.55, 24.71, 23.40, 21.89, 19.66, 18.70. HRESIMS m/z (pos): 733.2458 $C_{34}H_{41}N_2O_{16}$ (calcd. 733.2456).

4.1.13. ((4-(5,6-dihydroxy-4-oxo-7-(((2S,3S,4R,5R,6S)-3,4,5-trihydroxy-6-(methoxycarbonyl)tetrahydro-2H-pyran-2-yl)oxy)-4H-chromen-2-yl)phenoxy)carbonyl)-L-valyl-L-alloisoleucine (5l)

Yield 52.1%, light yellowish green solid. ^{1}H NMR (400 MHz, DMSO-d_6) δ 10.43 (s, 1H, 6-O*H*), 8.09 (d, J = 7.4 Hz, 1H, N*H*CHCOOH), 7.93 (d, J = 8.3 Hz, 2H, $C_{2'6'}$–2*H*), 7.80 (d, J = 8.1 Hz, 1H, N*H*CH-CH_3), 7.07 (s, 1H, C_3-*H*), 6.92 (d, J = 8.5 Hz, 2H, $C_{3'5'}$–2*H*), 6.88 (s, 1H, C_8-*H*), 5.31 – 5.27 (m, 1H, $C_{1''}$-*H*), 4.18 – 4.10 (m, 2H, C*H*CH_2CH$(CH_3)_2$, C*H*CH_3), 3.97 (t, J = 7.5 Hz, 1H, $C_{3''}$-*H*), 3.62 (s, 3H, COOC*H*$_3$), 1.98 (dt, J = 12.8, 6.0 Hz, 1H, C*H*$(CH_3)_2$), 1.73 – 1.72 (m, 1H, C*H*(CH_3)–CH_2CH_3), 1.38 (dt, J = 10.5, 5.2 Hz, 1H, CH(CH_3)C*H*CH_3), 1.21 – 1.12 (m, 1H, CH(CH_3)C*H*CH_3), 0.90 – 0.89 (m, 6H, CH(CH_3)$_2$), 0.82 – 0.79 (m, 6H, CH(CH_3)–CH_2CH_3). ^{13}C NMR (101 MHz, DMSO-d_6) δ 182.77, 173.31, 171.86, 169.67, 165.16, 162.00, 155.93, 153.97, 153.25, 129.20(2C), 124.27, 121.57, 116.58(2C), 106.08, 103.44, 100.03, 94.04, 75.84, 75.76, 73.28, 71.81, 60.56, 56.94, 55.44, 52.54, 36.75, 31.34, 25.22, 19.64, 18.73, 15.99, 11.90. HRESIMS m/z (pos): 733.2468 $C_{34}H_{41}N_2O_{16}$ (calcd. 733.2456).

4.2. Physiochemical property studies

For *in vitro* stability evaluation, 1 mg of the target compounds **5a–l** was dissolved in 20 μL DMSO to obtain stock solutions. Distilled water was then added to the above solutions to achieve a final concentration of 0.2 mg/mL. Subsequently, 200 μL of the diluted solution was added to 2 mL of plasma and intestinal fluid. The resulting solutions were maintained at 37 ± 0.5 °C in screw-capped vials in a water bath. The samples were withdrawn at appropriate time intervals, and analyzed by ultra-performance liquid chromatography-tandem mass spectrometry (UPLC–MS/MS). For the solubility test, 50 μL of distilled water was added to 2–4 mg of compounds **5a–l**. The solutions were ultrasonicated and filtered through a microporous membrane filter (0.45 μm). The saturated solutions were then diluted with distilled water to the corresponding multiple and the solubility for each compound was calculated using standard curves.

4.2.1. UPLC–MS/MS analysis conditions

UPLC analyses were performed utilizing a Waters ACQUITY UPLC instrument. The samples were separated on a BEH C l8 column (2.1 mm × 50 mm, 1.7 μm). The mobile phase consisted of acetonitrile containing 0.1% formic acid (A) and water containing 0.1% formic acid (B). The elution gradient was as follows: 10% A (0–2 min), 90% A (2–3 min), and 10% A (3 min). The mobile phase flow rate was set at 0.35 mL/min and the column temperature was 45 °C. The injection volume was 1 μL.

Mass spectrometry: All of the mass spectrometry experiments were carried out using a Waters ACQUITY TQD (triple quadrupole) spectrometer equipped with a Z-spray ESI source connected to the ACQUITY UPLC system. The acquisition parameters included collision gas, argon (Ar); nebulizing and drying gas, nitrogen (N_2); source temperature, 120 °C; desolvation temperature, 350 °C; cone gas flow, 50 l/h; desolvation gas flow, 650 l/h; collision gas flow, 0.16 mL/min; capillary voltage, 3.0 kV. The multi reaction monitor (MRM) mode was used. In the positive ion mode (ESI^+), the confirmation ion pairs were (m/z) 691.1 → 287(**5a**), 739.1 → 287 (**5b**), 721.1 → 287 (**5c**), 707.1 → 287 (**5d**), 705.2 → 287 (**5e**), 705.2 → 287 (**5f**), 691.1 → 287 (**5g**), 767.2 → 287 (**5 h**), 749.2 → 287 (**5i**), 735.1 → 287 (**5j**), 733.2 → 287 (**5k**), 733.2 → 287(**5l**). The cone voltage and collision voltage were in the range of 30–40 V. The UPLC-MS/MS results are summarized in Table 1.

4.3. Biological evaluation

Melatonin, dimethyl sulfoxide (DMSO), Lipofectamine™2000 transfection reagent, and 3-(4,5-dimethylthiazol-2-yl)-2,5-diphenyltetrazolium bromide (MTT) were purchased from Sigma-Aldrich (St. Louis, MO, USA). The Hoechst 33,342 nuclear staining assay kit and Annexin V/propidium iodide (PI) apoptosis detection kit were obtained from the Beyotime Institute of Biotechnology (BD Pharmingen™, USA). Anti-β-actin (abs132001) was purchased from Absin Bioscience Inc (Shanghai, China). Anti-caspase 3 (ab32351), anti-Bcl-2 (ab32124), and anti-Bax (ab32503) were obtained from Abcam (Cambridge, MA, USA). For the *in vitro* studies, compounds **5a-l** and scutellarin were dissolved in DMSO and formulated into 25 mM stock solutions.

4.3.1. Caco-2 cell permeability assay

4.3.1.1. Caco-2 cell culture. The Caco-2 cells were obtained from the Shanghai Institute of Material Medica (SIMM) and seeded onto Millicell™ Caco-2 plate at a density of 1.0 × 10^5 cells/cm^2. The Caco-2 cells were cultured in Dulbecco's Modified Eagle's Medium (DMEM) supplemented with 10% fetal bovine serum (FBS), 100 U/mL penicillin and streptomycin, 3.7 g/L $NaHCO_3$, and 1% L-glutamine (Gln). The cells were grown at 37 °C in a humidified incubator with an atmosphere of 5% CO_2.

4.3.1.2. Caco-2 cell-based permeability assay. Caco-2 cells were seeded at a density of approximately 1.0 × 10^5 cells/cm^2 on a 6-well Millicell™ plate and left to grow for 21 days until reaching confluence and differentiation. The integrity and transportation ability of the Caco-2 cell monolayer were examined by measuring the transepithelial electrical resistance (TEER) utilizing an epithelial voltohmmeter (Millicell-ERS electrical resistance system, Millipore, Bedford, MA). Inserts with TEER values ≥ 500 Ω cm^2 in the culture medium were selected for the transport experiments. On the 21st day, the Caco-2 cell monolayer was washed three times with a warm HBSS medium (pH = 7.4) and equilibrated in the same buffer. To determine the rate of the drug transport in the apical to basolateral direction, 0.4 mL of target compounds **5a-l** with a concentration of 1.5 × 10^{-4} M and scutellarin with a concentration of 2.0 × 10^{-4} M were added to the apical plate (AP), and the transport basolateral plate (BL) was filled with 0.6 mL of the HBSS buffer. Furthermore, to determine the transport rates in the basolateral to apical direction, 0.6 mL of the target compounds **5a-l** with a concentration of 1.5 × 10^{-4} M and scutellarin with a concentration of 2.0 × 10^{-4} M were added to the BL plate, and the filter wells (apical compartment, AP) were filled with 0.4 mL of the HBSS buffer. To establish the target compounds **5a-l** and scutellarin, 50 μL of the HBSS solution was taken from the AP or BL side and 150 μL of methanol was added to dilute the solution. The solution was subsequently centrifuged at 15,000 r/min for 10 min. A 10 μL aliquot of the supernatant solution was used for the UPLC–MS/MS assay according to the method described for the evaluation of the physiochemical properties. The obtained results are summarized in Table 2 and Fig. 1.

4.3.2. Cell culture and stable transfection

The Madin Darby Canine Kidney (MDCK) cells were obtained from the American Type Culture Collection (Manassas, VA, USA) and grown

in DMEM. The BCA protein quantitation reagent was purchased from Beijing Solarbio Science & Technology Co., Ltd. Lipofectamine™ 2000 was obtained from Invitrogen (Carlsbad, CA), while the anti-IgG antibody was purchased from Santa Cruz Biotechnology. The pcDNA3.1-hPepT1 plasmid was constructed by Beijing Bomeid Gene Technology Co., Ltd.

According to D'Mello et al. [35], the transfection protocol involved transfection of the MDCK cells with the pcDNA3.1-hPepT1 plasmid using Lipofectamine. Briefly, cells were seeded in 6-well plates at a density of 3×10^5 cells/well and incubated at 37 °C. After 24 h, the volume/mass ratio of Lipofectamine™ 2000:pcDNA3.1-hPepT1 (2:1) was transfected into the MDCK cells. After 48 h, G418 was added at the final concentration of 800 μg/ml and the cells were incubated for 2 weeks until antibiotic-resistant colonies were observed for the stably hPepT1-overexpressed mono-clone MDCK cells. Subsequently, hPepT1-MDCK stably transfected cells and MDCK were incubated with the typical substrate Gly-Sar (200 μM) at 37 °C for 5–50 min to identify the substrate uptake conditions.

4.3.2.1. Western blotting of the PepT1 expression. The above two kinds of cells were collected and lysed by radio immunoprecipitation assay (RIPA) buffer containing 1 mM phenylmethylsulfonyl fluoride (PMSF). The protein concentration was measured utilizing a BCA assay kit (Solarbio), the samples were separated by SDS-PAGE gel electrophoresis and transferred onto a polyvinylidene fluoride (PVDF) membrane. The employed primary antibodies included the anti-IgG antibody obtained from Santa Cruz Biotechnology.

4.3.3. Uptake of target compounds in the hPepT1 –MDCK cells

Based on the above analysis, the uptake mechanism for target compounds **5d**, **5g**, **5i**, and **5k** in the hPepT1-MDCK cells was evaluated at 30 min. Subsequently, the RIPA buffer (250 μL) was added to lyse the cells. The cell lysis solution was then centrifuged at 12,000*g* for 20 min at 4 °C and an aliquot of the supernatant (20 μL) was withdrawn for the determination of the protein levels using the BCA protein assay kit. In the second experiment, methanol (800 μL) was added to the cell lysis solution (200 μL) and the mixed solution was centrifuged twice at 12,000*g* for 20 min at 4 °C to precipitate the proteins. An aliquot of the supernatant solution (150 μL) was assayed using the UPLC-MS/MS method established for the evaluation of the physiochemical properties described above. All of the results are illustrated in Fig. 6 (A-C).

4.3.4. The lactate dehydrogenase (LDH) and malondialdehyde (MDA) assay

The PC12 cell line was obtained from Shanghai Cell Bank of the Chinese Academy of Sciences and was maintained at 37 °C in a medium supplemented with 5% heat-inactivated horse serum, 10% FBS, 100 U/mL penicillin, and 100 U/mL streptomycin.

After the cells were exposed to a 1000 μM solution of H_2O_2 in the presence of scutellarin for 24 h, the medium was collected, and the amount of LDH released by the cells was determined using an assay kit according to the manufacturer's protocol. The absorbance of the samples was read at 450 nm. The concentration of free MDA in the PC12 cells, i.e., the product formed due to peroxidation of the cell membrane, was assessed using an MDA kit according to the manufacturer's instructions. In brief, the assay was based on the reaction of MDA with thiobarbituric acid (TBA), forming stable thiobarbituric acid-reactive substances (TBARS), which absorb at 530 nm. The lipid peroxide level was expressed as nmol of MDA per mg of protein.

4.3.4.1. Cytotoxicity assay with Hoechst 33,342. The PC12 cells were grown in 6-well plates at a density of 8×10^4 cells/well. The cells were treated with varying concentrations of scutellarin and **5k** (2, 10, and 20 μM) for 24 h. Following this treatment, the cells were stained with Hoechst 33,342 for 10 min at 37 °C. The cells were then washed three times with PBS and the fluorescence images were acquired utilizing a fluorescence microscope. The condensation and fragmentation of nuclei was considered to be representative of apoptosis.

For the detection of intracellular reactive oxygen species (ROS), the cells were incubated with 10 μmol/L DCFH-DA at 37 °C for 30 min. Following washing twice with PBS, the cells were harvested and suspended in the same buffer. The fluorescence intensity was measured using a flow cytometer (BD).

4.3.4.2. Measurement of the mitochondrial membrane potential (ΔΨm). The mitochondrial membrane potential (ΔΨm) was determined using the Rhodamine 123 staining kit. The PC12 cells were grown in a 6-well plate at a density of 8×10^4 cells/well. The cells were then washed twice with PBS and incubated with 10 μg/ml Rhodamine 123 staining solution at 37 °C for 30 min in darkness. After washing away the unbound dye, the cells were fixed and observed under a fluorescence microscope.

4.3.4.3. Annexin V/PI staining assay. Apoptotic cells were analyzed utilizing the Annexin V (fluorescein isothiocyanate (FITC)-conjugated)/PI apoptosis kit (BD Pharmingen™, USA) by flow cytometry. The cells were subcultured in a 6-well plate at a density of 1×10^5 cells/well. Following treatment with varying concentrations of scutellarin and **5k** (2, 10, and 20 μM) for 24 h, the cells were harvested and resuspended in DMEM. Subsequently, the cells were incubated with 5 μL of Annexin V-FITC and 5 μL of PI for 15 min in the dark. After incubation, 400 μL of the buffer was added to each sample and the sample were analyzed using a flow cytometer (BD FACSCantoII). The percentage of cells residing in the lower right region of the scatter plot (early apoptotic cells) of Annexin V-FITC was calculated for comparison.

4.3.4.4. Cell cycle study. Based on the cell viability assay results, the PC12 cells were seeded into 6-well plates at a density of 8×10^4 cells/well and treated with 2, 10, and 20 μM of compound **5k** and 20 μM of Scu for 24 h. Following this treatment, the cells were digested with trypsin and centrifuged for 5 min (1500*g*). One mL of ice-cold PBS was then added to wash the centrifuged cells twice before fixing the cells with formalin for 30 min. Subsequently, the cellular membrane was broken using 0.5%Triton-X100 for 20 min at room temperature. The cells were then washed twice with PBS and collected by centrifugation. Propidium iodide (0.5 mL) was added to each tube to stain the cells, which were incubated in the dark at 37 °C for 30 min. The samples were then immediately analyzed with a flow cytometer (BD canto II plus).

4.3.4.5. Western blot analysis. The PC12 cells were subcultured in a 6-well plate at 2×10^5 cells/well and treated with varying concentrations of Scu and **5k** (2, 10, and 20 μM) for 24 h. The cells were harvested, washed twice with cold PBS, and then lysed in the RIPA extraction buffer containing 1 mM PMSF for 30 min on ice. The lysates were centrifuged at 12,000 rpm for 20 min at 4 °C. The supernatants were subsequently collected, and the protein concentrations were determined utilizing the Bio-rad Dc protein assay (Bio-rad Laboratories, CA, USA) using bovine serum albumin as the standard. Following SDS-PAGE, the protein samples were transferred onto a PVDF membrane. The employed primary antibodies included anti-caspase 3 (ab32351), anti-Bcl-2 (ab32124), anti-Bax (ab32503), and anti-β-actin (abs132001).

4.3.4.6. Molecular docking assay. The Schrodinger software was used for the molecular docking studies. The crystal structure of PepT1 (PDB ID: 4d2c) was obtained from the Protein Data Bank. Proteins were prepared using the Protein Preparation Wizard based on the force field OPLS (optimized potentials for liquid simulations) 2005. Compound **5k** was prepared using the LigPrep module to transform to the three-dimensional structure. The calculation was performed based on the Schrodinger extra precision (XP) mode and the structure with the

lowest energy was chosen as the final result. The details of the docking procedure were as follows: 1) Protein preparation: The PepT1 (PDB ID: 4d2c) protein was used as the docking template. The protein was processed and optimized using the Protein Preparation Wizard module of the Schrodinger software. 2) Ligand preparation: The ligand structure was drawn in ChemDraw, and the three dimensional structure of the molecule was transformed utilizing the LigPrep module to generate different conformations. 3) Molecular docking: The XP mode in the Schrodinger software was employed for molecular docking. Based on the binding mode of compound **5k** and the proteins, the docking conformation with the lowest docking energy was deemed as the final result.

4.3.5. In vivo neuroprotective characteristics evaluation

4.3.5.1. Animals. Four male Sprague-Dawley (SD) rats and 10–12 female rats were purchased from Tianqin Biotechnology Co., Ltd., Changsha City, Hunan Province. A total of 300 seven-day-old undenatured SD rat pups were used.

4.3.5.2. Hypoxic-ischemic encephalopathy (HIE) model. The HIE model of neonatal rats was established based on the experimental scheme of the rodent model established by Rice et al. [39]. Rat pups produced by mating between male and female SD rats were anesthetized with 2–4% isoflurane and their right carotid arteries were surgically ligated. Subsequently, the rat pups were returned to 37 ˚C for 1 h before being placed in a hypoxic chamber (8% oxygen-92% nitrogen) for 120 min. Pups treated by the sham operation were generated by ligating the ipsilateral carotid artery, but not subjecting them to hypoxic conditions.

4.3.5.3. Drug administration method. The rat pups were divided into five groups, i.e., the sham group (n = 6), HIE + vehicle group (n = 6), HIE + Scu (2.8 mg/kg) group (n = 6), HIE + **5k** (0.84 mg/kg) group (n = 6), and HIE + **5k** (2.8 mg/kg) group (n = 6). The pups were given an intraperitoneal injection of the tested drugs from the sixth day after birth. They were then treated with the HIE regimen, and the drugs were given for another 48 h by using the same route of administration.

4.3.5.4. TTC staining results. Cerebral infarct size was measured by 2,3,5-triphenyltetrazolium chloride (TTC) staining 48 h after HIE [40]. Briefly, the rats were decapitated after neurological evaluation, and the brains were removed quickly before being sliced into six uniform coronal sections (2 mm thickness each). The sections were stained with 2% TTC (Sigma-Aldrich) at room temperature for 15 min and then fixed in a 4% formaldehyde solution. The normal brain tissue was stained red, while the infarct areas were pale. The posterior surface of each slice was photographed and analyzed utilizing the ImageJ software. The infarct area was calculated as a percentage of the area of the contralateral hemisphere.

4.3.5.5. HE and Nissl staining results. After HIE rat pups were killed by deep anesthesia, the brains were perfused with heparinized physiologic saline, followed by 4% paraformaldehyde. The brains were removed and postfixed in 4% paraformaldehyde for 24 h before being embedded in paraffin. For measuring HE, the staining sections were cut and stained with hematoxylin and eosin 48 h after HIE, while for evaluating Nissl, the staining sections were stained with toluidine blue staining solution 4 weeks after HIE.

4.3.5.6. Neurological deficit score. The neurological deficit score of each rat pup 48 h after HIE was evaluated by an assessor, who was blinded to the treatment protocols. The neurological deficit was determined according to a five-point scale established by Bederson et al. [41], as follows: 0 = no neurological symptoms; 1 = unable to fully extend the front paw on the contralateral side; 2 = circling to the contralateral side; 3 = falling to the contralateral side; and 4 = unable to walk spontaneously.

4.3.5.7. Western blot analysis. After 48 h of HIE, six rat pups from each group were sacrificed and the brains on the same side of the embolization was immediately dissected and used for protein extraction. The rat pups' brains were homogenized in the RIPA buffer containing 1% protease and phosphatase inhibitor. The total proteins were collected from the supernatant after centrifugation at 12,000*g* for 15 min at 4 ˚C. Protein concentrations were measured using the Bradford protein assay (Bio-Rad Laboratories, Hercules, CA, USA). The samples were separated by the SDS-PAGE gel electrophoresis and transferred onto a PVDF membrane. The employed primary antibodies included rabbit anti-Amyloid Precursor Protein (ab32136) and anti-BACE1 (ab108394). The data was analyzed by the Quantity one software.

*4.4. Pharmacokinetic evaluation of scutellarin and its prodrug **5k***

The male SD rats (200 ~ 220 g) were divided into two groups, each with six rats, and fasted for 12 h prior to intravenous administration of scutellarin and **5k** at a dose of 10 mg/kg and 16 mg/kg, respectively. Blood samples (0.5 mL) were collected from suborbital vein into heparinized 1.5 mL centrifuge tubes at 0, 2, 5, 10, 30, 45, 60, and 120 min following drug administration. All of the blood samples were centrifuged at 15000*g* for 10 min after which the plasma samples were collected. The plasma concentrations of scutellarin and its prodrug **5k** were measured using the LC-MS/MS method (injection volume of 2 μL) described above for the evaluation of the physiochemical properties. The PK parameters were calculated utilizing DAS (version 2.0).

4.5. Statistical analysis

Data are shown as the mean ± standard deviation (SD). Statistical analysis was performed using one-way ANOVA or Student's *t*-test. A P-value of < 0.05 was considered to be statistically significant. GraphPad Prism was employed to perform the statistical analyses and generate the graphs.

Declaration of Competing Interest

None.

Acknowledgements

This work was supported by the grants from National Natural Science Foundation of China (NSFC Nos. 81260473 and 81460523), Projects of Guizhou Science and Technology Department (No. 2012-3013), and Excellent Youth Scientific Talents Foundation of Guizhou Province (No. 2013-45).

Appendix A. Supplementary material

Supplementary data to this article can be found online at https://doi.org/10.1016/j.bioorg.2020.103980.

References

[1] M. Fotuhi, V. Hachinski, P.J. Whitehouse, Changing perspectives regarding late-life dementia, Nat. Rev. Neurol. 5 (12) (2009) 649–658.
[2] R.C. Vannucci, J.R. Connor, D.T. Mauger, et al., Rat model of perinatal hypoxic-ischemic brain damage, Neurosci. Res. 55 (2) (1999) 158–163.
[3] S. Adhikari, K.S. Rao, Neurodevelopmental outcome of term infants with perinatal asphyxia with hypoxic ischemic encephalopathy stage II, Brain Dev. 39 (2) (2017) 107–111.
[4] C. McLean, D. Ferriero, Mechanisms of hypoxic-ischemic injury in the term infant, Semin. Perinatol. 28 (6) (2004) 425–432.
[5] J.M. Lorenz, D.E. Wooliever, J.R. Jetton, et al., A quantitative review of mortality and developmental disability in extremely premature newborns, Arch. Pediatr.

Adolesc. Med. 152 (5) (1998) 425–435.
[6] D. Doycheva, G. Shih, H. Chen, et al., Granulocytecolony stimulating in combination with stem cell factor confers greater neuroprotection after hypoxic-ischemic brain damage in the neonatal rats than a solitary treatment, Transl. Stroke Res. 4 (2) (2013) 171–178.
[7] J. Shetty, Neonatal seizures in hypoxic-ischemic encephalopathy–risks and benefits of anticonvulsant therapy, Dev. Med. Child Neurol. 57 (2015) 40–43.
[8] B.J. Dixon, C. Reis, W.M. Ho, et al., Neuroprotective strategies after neonatal hypoxic ischemic encephalopathy, Int. J. Mol. Sci. 16 (9) (2015) 22368–22401.
[9] L. Wang, Q. Ma, Clinical benefits and pharmacology of scutellarin: a comprehensive review, Pharmacol. Ther. 190 (2018) 105–127.
[10] J. Zhu, L. Chen, Y. Qi, et al., Protective effects of Hand.- Mazz. (EBHM) extract in retinal neurodegeneration models, Mol. Vis. 24(2018) 315–325.
[11] H. Liu, X. Yang, R. Tang, et al., Effect of scutellarin on nitric oxide production in early stages of neuron damage induced by hydrogen peroxide, Pharmacol. Res. 51 (3) (2005) 205–210.
[12] H. Hong, G.Q. Liu, Scutellarin attenuates oxidative glutamate toxicity in PC12 cells, Planta Med. 70 (5) (2004) 427–431.
[13] L.L. Guo, Z.Z. Guan, Y.L. Wang, Scutellarin protects against Abeta-induced learning and memory deficits in rats: involvement of nicotinic acetylcholine receptors and cholinesterase, Acta Pharmacol. Sin. 32 (12) (2011) 1446–1453.
[14] H.F. Zhang, X.M. Hu, L.X. Wang, et al., Protective effects of scutellarin against cerebral ischemia in rats: Evidence for inhibition of the apoptosis-inducing factor pathway, Planta Med. 75 (2) (2009) 121–126.
[15] L. Qian, M. Shen, H. Tang, et al., Synthesis and protective effect of scutellarein on focal cerebral ischemia/reperfusion in rats, Molecules 17 (9) (2012) 10667–10674.
[16] Y. Yuan, H. Zha, P. Rangarajan, et al., Anti-inflammatory effects of Edaravone and Scutellarin in activated microglia in experimentally induced ischemia injury in rats and in BV-2 microglia, BMC Neurosci. 15 (2014) 125.
[17] L.L. Guo, Z.Z. Guan, Y. Huang, et al., The neurotoxicity of beta-amyloid peptide toward rat brain is associated with enhanced oxidative stress, inflammation and apoptosis, all of which can be attenuated by scutellarin, Exp. Toxicol. Pathol. 65 (5) (2013) 579–584.
[18] J.W. Shin, K.J. Kweon, D.K. Kim, et al., Scutellarin Ameliorates Learning and Memory Deficit via Suppressing β-Amyloid Formation and Microglial Activation in Rats with Chronic Cerebral Hypoperfusion, Am. J. Chin. Med. 46 (6) (2018) 1203–1223.
[19] Y.J. Gong, J.X. Wang, Y. Zhang, et al., Intestinal lymphatic transport of breviscapine orally administered in rat. Acta. Pharm. Sin. 46(10)(2011)1262-1267.
[20] X. Chen, L. Cui, X. Duan, et al., Pharmacokinetics and metabolism of the flavonoid scutellarin in humans after a single oral administration, Drug Metab Dispos 34 (8) (2006) 1345–1352.
[21] X.M. Hu, M.M. Zhou, X.M. Hu, et al., Neuroprotective effects of scutellarin on rat neuronal damage induced by cerebral ischemia/reperfusion, Acta Pharmacol. Sin. 26 (12) (2005) 1454–1459.
[22] Y. Wang, H. Ao, Z. Qian, et al., Intestinal transport of scutellarein and scutellarin and first-pass metabolism by UDPglucuronosyltransferase-mediated glucuronidation of scutellarein and hydrolysis of scutellarin, Xenobiotica 41 (7) (2011) 538–548.
[23] W. Cong, L. Shen, D. Xu, et al., Solid dispersion tablets of breviscapine with polyvinylpyrrolidone K30 for improved dissolution and bioavailability to commercial breviscapine tablets in beagle dogs, Eur. J. Drug Metab. Pharmacokinet. 39 (3) (2014) 203–210.
[24] F. Cao, J. Jia, Z. Yin, et al., Ethylene glycol-linked amino acid diester prodrugs of oleanolic acid for PepT1-mediated transport: synthesis, intestinal permeability and pharmacokinetics, Mol. Pharm. 9 (8) (2012) 2127–2135.
[25] Y. Gong, X. Wu, T. Wang, et al., Targeting PEPT1: A novel strategy to improve the antitumor efcacy of Doxorubicin in human hepatocellular carcinoma therapy, Oncotarget 8 (25) (2017) 40454–40468.
[26] B.S. Anand, J. Patel, A.K. Mitra, Interactions of the dipeptide ester prodrugs of acyclovir with the intestinal oligopeptide transporter: competitive inhibition of glycylsarcosine transport in human intestinal cell line-Caco-2, J. Pharmacol. Exp. Ther. 304 (2) (2003) 781–791.
[27] L. Fang, M. Wang, S. Gou, et al., Combination of amino acid/dipeptide with nitric oxide donating oleanolic acid derivatives as PepT1 targeting antitumor prodrugs, J. Med. Chem. 57 (3) (2014) 1116–1120.
[28] L.H. Zhang, L. Zhang, T. Luo, Synthesis and evaluation of a dipeptide drug conjugate library as substrates for PEPT1, ACS Comb. Sci. 14 (2012) 108–114.
[29] G. Ni, Y. Tang, M. Li, et al., Synthesis of Scutellarein Derivatives with a Long Aliphatic Chain and Their Biological Evaluation against Human Cancer Cells. Molecules. 23(2)(2018) pii: E310.
[30] F. Cao, J.X. Guo, Q.N. Ping, et al., Prodrugs of scutellarin: ethyl, benzyl and N, N-diethylglycolamide ester synthesis, physicochemical properties, intestinal metabolism and oral bioavailability in the rats, Eur. J. Pharm. Sci. 29 (5) (2006) 385–393.
[31] Z.X. Dong, Z.H. Shi, N.G. Li, et al., Design, Synthesis, and Biological Evaluation of Scutellarein Derivatives Based on Scutellarin Metabolic Mechanism In Vivo. Chem. Biol. Drug Des. 87(6)(2016)946-957.
[32] C. Chu, C.T. Okamoto, S.F. Hamm-Alvarez, et al., Stable transfection of MDCK cells with epitope-tagged human PepT1, Pharm. Res. 21 (11) (2004) 1970–1973.
[33] Y. Fujisawa, R. Tateoka, T. Nara, et al., The extracellular pH dependency of transport activity by human oligopeptide transporter 1 (hPEPT1) expressed stably in Chinese hamster ovary (CHO) cells: a reason for the bell-shaped activity versus pH, Biol. Pharm. Bull. 29 (5) (2006) 997–1005.
[34] Y. Wang, R. Wang, Y. Wang, et al., Ginkgo biloba extract mitigates liver fbrosis and apoptosis by regulating p38 MAPK, NF-κB/IκBα, and Bcl-2/Bax signaling, Drug Des. Devel. Ther. 9 (2015) 6303–6317.
[35] S.R. D'Mello, C.Y. Kuan, R.A. Flavell, et al., Caspase-3 is required for apoptosis-associated DNA fragmentation but not for cell death in neurons deprived of potassium. J. Neurosci. Res. 59(1)(2000)24-31.
[36] R. Vassar, B.D. Bennett, S. Babu-Khan, et al., Beta-secretase cleavage of Alzheimer's amyloid precursor protein by the transmembrane aspartic protease BACE, Science. 286 (5440) (1999) 735–741.
[37] X. Sun, G. He, H. Qing, et al., Hypoxia facilitates Alzheimer's disease pathogenesis by up-regulating BACE1 gene expression, Proc. Natl. Acad. Sci. USA 103 (49) (2006) 18727–18732.
[38] J.A. Bonds, A. Shetti, A. Bheri, et al., Depletion of Caveolin-1 in Type-2 Diabetes Model Induces Alzheimer's disease Pathology Precursors. J. Neurosci. 39(43)(2019) 8576-8583.
[39] J.E. Rice 3rd, R.C. Vannucci, J.B. Brierley, The influence of immaturity on hypoxic-ischemic brain damage in the rat, Ann Neurol. 9 (2) (1981) 131–141.
[40] J.B. Bederson, L.H. Pitts, M. Tsuji, et al., Rat middle cerebral artery occlusion: evaluation of the model and development of a neurologic examination. Stroke. 17(3)(1986) 472-476.
[41] L. Ye, Z. Feng, D. Doycheva, et al., CpG-ODN exerts a neuroprotective effect via the TLR9/pAMPK signaling pathway by activation of autophagy in a neonatal HIE rat model, Exp. Neurol. 301 (2018) 70–80.